HEAT TRANSFER COEFFICIENTS OF PARTICULATE IN TUBULAR HEAT EXCHANGERS

A Thesis
Presented to
The Academic Faculty

by

Clayton M. Nguyen

In Partial Fulfillment
Of the Requirements for the Degree
Master of Science in the
George W. Woodruff School of Mechanical Engineering

Georgia Institute of Technology

August 2015

HEAT TRANSFER COEFFICIENTS OF PARTICULATE IN TUBULAR HEAT EXCHANGERS

Approved by:

Dr. Sheldon Jeter, Advisor
School of Mechanical Engineering
Georgia Institute of Technology

Dr. Said Abdel-Khalik
School of Mechanical Engineering
Georgia Institute of Technology

Dr. Peter Loutzenhiser
School of Mechanical Engineering
Georgia Institute of Technology

Date Approved: 7/23/2015

ACKNOWLEDGEMENTS

I would like to thank everyone who has helped with and encouraged me through this thesis. There are many who have freely dedicated their time to help me with this thesis and teach me valuable skills.

I would like to thank Dr. Sheldon Jeter for being my advisor. It is through him that I have developed many of my skills over the past few years and without whom this thesis would not have been possible. Dr. Said Abdel-Khalik has also been a great source of guidance and role model as a researcher. Additionally I would like to thank Dr. Peter Loutzenhiser for being a committee member and a research collaborator.

For their help in providing technical knowledge, and skills I also thank Dennis Sadowski and Matthew Golob. Additionally I'd like to thank my fellow classmates Robbie, Ryan, Jonathan, Max, Maggie, Kenzo, Kyle and Ahmad for their support these past few years.

Finally I'd like to thank my friends and family for their words of encouragement and understanding throughout this undertaking.

TABLE OF CONTENTS

LIST OF TABLES

LIST OF FIGURES

LIST OF ABBREVIATIONS

ATL	Atlanta industrial sand
CSP	Concentrated Solar Power
DAQ	Data Acquisition
DSC	Digital Scanning Calorimeter
HTF	Heat Transfer Fluid
ID50-K	50 mesh intermediate density proppant
NIST	National Institute of Science and Technology
PFHX	Particle to working fluid heat exchanger
PHR	Particle Heating Receiver
PRT	Platinum resistance thermometer
RTD	resistance temperature detectors
RWS	Riyadh white sand
SMD	Sauter Mean Diameter
TC	Thermocouple
UA	Statistical Uncertainty
UB	Uncertainty due to system bias

LIST OF SYMBOLS AND NOMENCLATURE

μ	Dynamic viscosity
A_{bare}	Surface area of bare tube
A_{base}	Base surface area of finned tube
A_{fin}	Fin surface area
$A_{fin,tube}$	Finned tube area for a single tube
$A_{surface,box}$	Outside surface area of heat exchanger box
c_{fin}	Parameter used for calculating fin efficiency
C_g	Constant parameter for Grimison correlation
C_h	Constant parameter for Hilpert correlation
c_p	Specific heat
C_z, C_{z2}	Constant parameter for Zhukauskas correlation
D	Hydraulic diameter
d_p	Particle diameter
D_o	Tube diameter
G_{max}	Maximum flux speed
$\bar{h}$	Heat transfer coefficient
h_{air}	Air Heat transfer coefficient
$h_{apparent}$	Apparent heat transfer coefficient
$h_{average}$	Average heat transfer coefficient
$h_{effective}$	Effective heat transfer coefficient
k_{air}	Conductivity of air
k_{fin}	conductivity of fin
k_{part}	conductivity of particulate
$LMTD$	log mean temperature difference
L	Length of tube
m	Parameter used for calculating fin efficiency
$\dot{m}$	mass flow rate
m_h	constant parameter for Hilpert correlation
N_{fins}	Number of fins
Nu	Nusselt number
$\overline{Nu}_{Bank,n\geq10}$	Nusselt number for a bank of tubes with > 10 rows
Pr	Prandtl number
Pr_s	Prandtl number at STP
$\dot{Q}_{tube}$	Power into one heater
$\dot{Q}_{loss}$	Overall Heat Loss
$\dot{Q}$	Overall heat input
r_1	Radius of finned tube base
r_2	Fin radius

r_{2c}	Corrected fin radius
R_{air}	Thermal resistance of air
R_{part}	Thermal resistance of particles
R_{wall}	Thermal resistance of heat exchanger wall
Re	Reynolds number
$\text{Re}_{D,\text{max}}$	Reynolds number max
SMD	Sauter Mean Diameter
t	Fin thickness
$T_{\text{air,in}}$	Inlet air temperature
$T_{\text{air,out}}$	outlet air temperature
T_{amb}	Ambient temperature
$T_{\text{heater,down}}$	Downstream heater temperature
$T_{\text{heater, up}}$	Upstream heater temperature
$T_{\text{par,avg}}$	Average particle temperature
$T_{\text{par,inlet}}$	Inlet particle temperature
$T_{\text{par,outlet}}$	Outlet particle temperature
U	thermal conductivity
w_i	Weight of particle
ε	Fin effectiveness
η_{fin}	Fin efficiency

SUMMARY

This experimental study explores the heat transfer from heated bare and finned tubular surfaces to particulates in packed bed cross flow. The results from this experiment will be used to help select the type of particulates that will be used. Additionally, these results will assist in estimating heat transfer in prototype and commercial particle to fluid heat exchangers (PFHX).

This research is part of larger effort in the use of particulates in concentrating solar power technology. These solid particles are heated by concentrated sunlight to very high temperatures at which they are a suitable heat source for various thermal power and thermochemical cycles. Furthermore, one of the advantages of this concept is the ability to store thermal energy in the solid particles at relatively low cost. However, an important feature of any Particle Heat Receiver (PHR) system is the PFHX, which is the interface between the solar energy system and the thermal power or chemical system. In order to create this system material data is needed for the design and optimization of this PFHX.

The paper focuses on the heat transfer properties of particulates to solid surfaces under plug flow conditions. The particulates will be evaluated for three grain sizes of sand and two grain sizes of proppants. These two materials will be tested at one, five and ten millimeters per second in order to see how the various flow rates, which will be required for different loads, will affect the heat transfer coefficient. Finally the heat transfer coefficient will also be evaluated for both finned and non-finned heat exchangers to see the effect that changes in the surface geometry and surface area have on the heat transfer coefficient. The heat transfer coefficient will help determine the appropriate material that will be used in the PHR system.

CHAPTER 1

INTRODUCTION

This thesis explores the use of particulates in solar energy systems. It is part of a greater body of work pertaining to the creation of a concentrating solar power (CSP) plant that uses particulates as the thermal fluid. This paper will focus on the heat exchanger unit and its interaction with various types of particulates. Standard CSP plants use a heat transfer fluid to transfer the heat from the solar collector field to the power cycle. There are typically two types of CSP fields, the first is the use of parabolic troughs and the second has a solar power tower in a field of heliostats. The solar power tower is the primary focus of this project. Modern power towers currently use molten salts as the heat transfer fluid (HTF) however a major disadvantage to this is the high costs and technical problems when using molten salts a thermal storage unit. In addition, the high vapor pressures needed for highly reinforced storage facilities add substantial costs to the system.

The major advantage of particulates for CSP technology is its use in energy storage. Currently molten salts are limited due to the high temperatures at which they freeze. Freezing temperatures range between 80 to 200° Celsius (1). Once frozen, the molten salts will completely obstruct the pipeline, creating numerous difficulties in restoring the liquid flow through the system. In addition to minimum low temperature operating restrictions, molten salts also begin to decompose at temperatures around 550° C leading to an even more corrosive environment that is dangerous to the system (2).

In addition to the ease of storage, the solid particulates that are being considered are to be used at higher temperatures then modern salts. These higher temperatures, while creating some material considerations, allow for higher power cycle efficiencies.

The proposed technology will also reduce the levelized cost of electricity (LCOE) of solar technology. Not only is the thermal medium cheaper than molten salts; there is also balance of plant savings. Molten salts are a highly corrosive material and as such the pumps, pipeline, and the heat exchanger use more expensive materials to ensure that the system can operate under those conditions. In addition to concerns with corrosion, the molten salts are also pressurized requiring further capital.

Unfortunately the use of particulates as a thermal medium is still a relatively new concept in CSP technology, studies in how the particles will interact with the heating receiver, the heat exchanger and the transport mechanisms need to be studied. This paper is concerned with the particulate heat transfer coefficient for tube and finned tubed heat exchangers.

1.1 **Heat Exchanger**

The solar power tower will have a heat exchanger unit that interfaces directly with the power cycle. The configuration that is being considered is a finned tube design due to its proven worth as a fluid heat exchanger. The heat exchanger in the tower is 1m x 1m x 1m. To study the heat transfer properties for this system a small scale lab heat exchanger has been created. The device studies particulate flow using two separate configurations. The first is a simple bare tubed configuration consisting of nine electric heaters. The second configuration uses a finned tube that snugly fits over the electric heaters to form the finned heat exchanger. The large scale version uses the same type of tubing. The finned tubing is 101.6 mm long, has 3 fins per mm and is made

of stainless steel. Each finned tube has an inner diameter of ~15.875mm and snugly fits the heaters. The heat exchanger is part of a high temperature power cycle, the most likely option for this would be a supercritical CO2 cycle which can operate at the temperatures that the project hopes to achieve, approximately 700°C. Though the heat exchanger geometry is of significant importance, the focus of this paper will pertain to the heat transfer properties of the particulates.

1.2 Particulates

There is a wide variety of particulates that will be studied in this thesis. The selection criteria are based on the particles' size, uniformity and absorptivity. As a commonly, available material silica sands are one of the main categories of material that will be used. In addition to sand, alumina beads are considered for use due to their dark coloring and high degree of particle size uniformity. This thesis will focus on discovering the heat transfer coefficient from the surface of the heat exchanger to the thermal medium, which is a dense or packed bed of particulates and interstitial air in cross flow.

CHAPTER 2

LITERATURE REVIEW

As this thesis covers the heat transfer particles of particulates, a literature review has been conducted in common modes of particulate heat transfer. This knowledge provides a framework of knowledge within which the experimental values can be evaluated and compared. The review will cover both particulate heat exchanger and thermal storage methods. The primary method of heat transfer for this experiment will be particle-particle heat transfer and particle-wall heat transfer. To provide a basis of knowledge the heat transfer coefficients of fluidized, slug and free flowing particulate flow will be examined.

In addition to a review of particle to particle heat transfer, the heat transfer of air over cylinders will also be reviewed. The air heat transfer literature will validate the experimental apparatus. To cover both possible heat transfer regimes, heat transfer over a single tube and a staggered bank of tubes are observed.

2.1 Heat Transfer in Packed Beds

Heat transfer in packed beds is the primary focus of this literature review due to its direct applicability to this work. This type of flow is characterized by its restricted movement through a confined area as opposed to free flow over a surface. Another name for this type of restricted flow is plug or slug flow.

Achenbach (3) has conducted studies into the “Heat and Flow Characteristics of Packed Beds”. In his paper he presents correlations that predict the heat transfer, pressure drop and effective conductivity of packed beds. These studies are conducted using a single heated bead

surrounded by particles and account for both stagnant and steaming gas flows. The results on effective conductivity are used for the slug flow experiments to assist in estimating the heat loss.

The research on , “Heat Transfer in Moving Beds with a Stagnant Interstitial Gas” by Molerus (4), deals with geometry that is a close match with the PFHX. Unfortunately, his experiment the paper does not attempt to calculate the heat transfer coefficient. However it does provide insight into mode of heat transfer. Molerus studies hard materials, treated as inelastic particles. His findings assume that the thermal resistance of the particulate is insignificant in comparison to the resistance of the air. Overall he concludes that the most significant factor in this type of heat transfer is the heat surface to moving bed contact resistance.

Vargas (5) experimentally and computationally investigated heat transfer for a packed bed of particles using cylindrical heating elements. The elements, particulates and void spaces were modeled using the discrete element methods with a fine enough resolution that the bed heterogeneities are included in the modeling efforts. One of the major concerns of his work is the presence of stress chains. Stress chains are networks of particles that are sheared causing deformation and increased heat transfer across the chain relative to areas that are not under shear. Vargas (6) also proceeds to show that his work encapsulates stagnant interstitial fluids. His thesis studies “granular systems under static and slow flow conditions” (5) for rotating drum flow. In that experiment he found the heat transfer coefficient to be 100-200 W/m^2-K. In addition to the experimental work he has conducted Vargas (7) has also created a discrete element model for evaluating such systems. He determined that the heat transport process depends on shear rate with conduction dominating the lower shear rates and convection dominating the higher shear rates.

Denloye (8) conducted a packed flowing bed where the particles flow along a heated surface. This experiment was conducted for particles ranging from 160 to 2370 micrometers. He concluded that the "surface heat transfer coefficient increases with decreasing particle residence time, decreasing particle size and with increasing gas thermal conductivity". While his experiment primarily investigated residence time, estimates from the PFHX experiment predicts a heat transfer coefficient on the order of 150 W/m^2-K for sand.

Brinn's (9) experiment is perhaps the most similar to the experiment that will be conducted in this paper. Brinn studied the heat transfer of silica sand as a settled bed through a pipe. The pipe has an outer layer which is used for both parallel and counter flow cooling/heating. The resulting heat transfer coefficient values range from 40-120W/m^2-K. In addition, Brinn observed that for his experiment the specific heat varies significantly over a range of temperature from 20 to 150°C. In addition, due to temperature striations within the material the outlet temperature had to be measured calorimetrically, which will be an item of significant concern within this thesis.

The most relevant work to this thesis is Alrished's (10) work on packed a packed bed bare tube heat exchanger. His work leads directly into the work that will be completed in this thesis and is further explained in Chapter 3. The heat transfer coefficients he obtained were between 40-120 W/m^2-K for speeds for 1mm/s – 3mm/s.

In addition to Abdul-Aziz's work, there has been previous work on this experiment using the current apparatus by Nguyen (11). The experiment conducts a preliminary evaluation of the data obtained in this thesis and has since been updated. Previously, the specific heats were measured by a transient hot wire device. The transient hot wire deceive is a KD2PRO from Decagon Devices (12) and is typically used to measure fluids and solid blocks of material. In

addition, a full error propagation analysis had yet to be performed on the data. From the preliminary work heat transfer coefficients of 80-140 W/m^2-K for flow speeds of 3mm/s – 10mm/s should be expected.

While the work conducted is most similar to a packed bed, other common types of particulate heat transfer will also be reviewed. This is to provide upper bound of expected heat transfer values for particulate heat transfer.

2.2 Heat Transfer in Fluidized Beds

In comparison to packed beds, fluidized beds entrain the particulates in a fluid causing the mixture to act as a fluid. The presence of a moving interstitial fluid causes an increase in particulate mixing minimizing the striations seen in Brinn's work. Additionally, the interstitial fluids movement increases the fluid-particulate heat transfer in comparison to the stagnant air present in packed beds.

A fluidized bed heat exchanger studied by Honda (13) uses similar heat exchanger geometry to the experiment in this study, though the particles are orders of magnitude larger. The flow in this experiment was examined using a thermal neutron radiograph system, which would be essential for furthering the scope of this project. As it stands the paper shows that fluidized beds using similar heat exchanger configurations will have a heat transfer of approximately 100 – 300 W/m^2-K. These results also show that the geometry has significant effects on the heat transfer coefficient.

According to Natale (14) Fluidized beds have typical heat transfer coefficients of 100-1000 W/m^2-K. For particulates (polymers, ballotini, corundum, carborundum and quartz sand) with a superficial velocity above 0.04 m/s the particles quickly reach approximately 80% of their

maximum values which ranges from 200- 600 W/m^2-K. These particulates are an order of magnitude smaller than those used in the plug flow experiment.

While this thesis is concerned with HTF in moving packed beds, the literature review above was presented primarily to establish a useful but far upper bound on the performance to be expected from moving packed beds.

2.3 Heat Transfer of Free Flowing Particulates

In a thesis by Golob (15), the heat transfer of particles flowing over a flat plate are experimentally determined. In the experiment particulates are dropped onto a series of heated flat plates angled at 45 degrees. For silica sands, the heat transfer coefficients ranges from 289-649 W/m^2-K depending on the average grain size. Similar to the situation with fluidized beds, this result for flowing beds is important to cite as another closer upper bound to heat transfer performance be expected from slowly moving packed beds.

2.4 Heat Transfer of Air Through a Tube Bank

Literature values are also used to validate the heat exchanger with air as a thermal fluid. These values will be used to validate the experiment and ensure that realistic values are obtained. The heat transfer property of air is expected to closely simulate either external air flow over a bank of tubes or air flowing over a single tube. Each the correlations presented uses empirical data as their basis.

For the heat transfer over a bank of tube the tubes are arranged in staggered fashion. The basis of this review of tube bank heat transfer is formed by Grimison (16), who provides a correlation for the average heat transfer coefficient for entire tube bundles of 10 or more rows.

This correlation ranges applies for $2000 < \mathrm{Re}_{D,\max} < 40{,}000$ with a $\mathrm{Pr} \geq 0.7$. The correlation is of the form:

$$\overline{Nu}_{Bank,n\geq 10} = C_g \, \mathrm{Re}_{D,\max}^{m} \qquad \textbf{2-1}$$

C_1 and m are constants for correlations based on different geometries.

When a fluid is used as the thermal medium the initial row of the heat exchanger generates turbulence in the flow increasing the heat transfer coefficient of air around the rows behind it. As such, the additional tubes cause an increase in the average heat transfer coefficient. A secondary correction factor can then be applied for tube banks with less than 10 rows. Since the heat exchanger in this experiment only has 3 rows the equation is modified to the form:

$$Nu_D = \frac{\bar{h}D}{k} = 1.13 \mathrm{C_g Re_{D,max} Pr}^{1/3} \qquad \textbf{2-2}$$

Zhukauskas provides another correlation incorporating more recent reuslts:

$$Nu_D = \frac{\bar{h}D}{k} = \mathrm{C_{z2}\, C_z Re_{D,Max}}^{\mathrm{m}} \mathrm{Pr}^{0.36} \left(\frac{\mathrm{Pr}}{\mathrm{Pr_s}} \right)^{1/4} \qquad \textbf{2-3}$$

The Zhukauskas correlation applies for $1000 < \mathrm{Re}_{D,\max} < 2\times10^{6}$. In addition, the standard ASHRAE handbook references the following correlation by Colburn under turbulent conditions:

$$Nu_D = \frac{\bar{h}D}{k} = 0.33 \left(\frac{\mathrm{G_{max} D_o}}{\mu} \right)^{0.6} \left(\frac{\mu c_p}{\mathrm{k}} \right)^{1/3} \qquad \textbf{2-4}$$

These correlations provide the expected experimental values assuming that the heat exchanger is acting as a tube bank. In the current experiment the Reynolds Number (defined for the tube diameter and the maximum velocity prevailing in the gap between tubes) is 7,100, which is well within the range of all the correlations.

2.5 Heat Transfer over a Single Tube

To provide a lower bound to the expected values the heat transfer of a single tube is also examined. As empirical evidence, the correlations created by Hilpert, Churchill and Zhukauskas (16), are used to examine the heat transfer coefficient for a single tube. In addition, the commonly used correlation from the ASHRAE handbook has also been included. The ASHRAE correlation combines a number of different data sets, including Hilpert's data set which covers the largest range of the parameters (17). In the current experiment the Reynolds Number (defined for the tube diameter and the upstream, free-stream velocity) is 4,200, which is well within the range of all the correlations.

Table 1: Empirical Correlations for the Heat Transfer Coefficient of Air

Source	Correlation	Valid Range
Hilpert	$Nu_D = \frac{\bar{h}D}{k} = C\,\mathrm{Re}_D^m\,\mathrm{Pr}^{1/3}$	$0.4 < \mathrm{Re_D} < 400{,}000$
ASHRAE	$Nu_D = \frac{\bar{h}D}{k} = 0.24\left(\frac{\mathrm{G\ D_o}}{\mu}\right)^{0.6^{1/3}}$	Air Only $1000 < \mathrm{Re_D} < 50{,}000$
Churchill	$Nu_D = \frac{\bar{h}D}{k} = 0.3 + \frac{.62\sqrt{\mathrm{Re_D}}\,\mathrm{Pr}^{1/3}}{(1+(.4/\mathrm{Pr})^{2/3})^{1/4}}\left(1+\left(\frac{\mathrm{Re}}{282000}\right)^{5/8}\right)^{4/5}$	$\mathrm{Re_D Pr} > 0.2$
Zhukauskas	$Nu_D = \frac{\bar{h}D}{k} = 0.51\sqrt{\mathrm{Re_D}}\,\mathrm{Pr}^{0.37}\left(\frac{\mathrm{Pr}}{\mathrm{Pr_s}}\right)^{1/4}$	$0.7 < \mathrm{Pr} < 500$ $1 < \mathrm{Re_D} < 10^6$

2.6 Background Literature

To conduct this experiment a constant flow rate is needed. L. Staron, et. al (18) has conducted research to granular silos which is used to support the Beverloo scaling factor. The literature shows that in granular flow the flow rate is dependent on the discharge area and is

independent of the head above the discharge. This is essential in the creation of the flow controller for the heat exchanger system.

One of the most important parameters for this experiment will be the calculation of an outlet temperature using the specific heat of the particles. To obtain the specific heat value the Kopp-Neumann Law is used. The original work was done in 1865 by Kopp (19) whose work has since been further refined. The latest literature, by Leitner (20), has been a study used to validate the specific heat value at different temperature. This body of work finds that at ambient temperatures there is approximately a 3% error in the estimation at near ambient, and 4-6% error as the temperatures approach 2000 K.

2.7 Literature Summary

The background in the literature value ultimately provides a basis through which this experiment is conducted. The following table provides a quick summary of the expected values for each type of flow in the literature review.

Table 2: Literature Review Heat Transfer Coefficient Summary

Authors	**Description of Flow**	**Heat Transfer Coefficients (W/m2-K)**
Golob (15)	Free Flow	289-649
Alrished (10)	Packed Bed	40-120
Brinn (9)	Cylindrical Packed Bed	100-200
Nguyen (11)	Packed Bed	80-140
Honda (13)	Fluidized Bed	100-300
Natale (14)	Fluidized Bed	100-1000

For the most applicable situation related to the current geometry, Brinn's heat transfer experiment in a packed bed, the expected values are 100 – 200 W/m^2-K. Otherwise the

preliminary work, as well as previous work done by Alrished suggest values between 40-120 W/m^2-K. To validate the model classic heat transfer correlations have for fluids been reviewed, selected and presented in sections 2.4 and 2.5.

CHAPTER 3

EXPERIMENTAL SYSTEM

This experimental system is designed to simulate a heat exchanger but does not directly measure the heat transfer of a heat exchanger system. Instead the purpose of this system is to find the heat transfer properties from a heat exchanger surface to its thermal medium, particulate in this case. The resultant heat transfer coefficient of the particulates will be analogous to the convection coefficient for fluids.

To test the particulates, several apparatuses have been used to recirculate particulates through the heat exchanger. Described in section 3.1, Alrished created the first iteration of this project using a conveyor-scoop system to raise the particles. This chapter describes the changes to the test apparatus, focusing on changes to the heat exchanger and the use of Olds Elevator as the recirculation loop. In addition the test articles will be evaluated for various material properties and the considerations that need to be made depending on the type of material used. Finally, this chapter will cover the instrumentation used to conduct the experiment.

3.1 Experimental Background

This experiment is an extension of one conducted by Abdul-Aziz Alrished (21). The original experiment investigated the characteristics of the bulk flow of sand for finned and bare tube heat exchangers. The apparatus consisted of three main parts a sand hopper, a heat exchanger test section and a set of movable grates to control the sand flow. A particulate conveyor system is used to fill the sand hopper. The sand hopper then pours into the heat exchanger test section that includes a small reservoir to ensure that the heat exchanger retains enough sand for plug flow. Alrished's experiment focused on sand velocities of 1 mm/s and 3

mm/s while this thesis will focus on sand velocities of 3 mm/s to 10 mm/s. The materials studied were olivine and silica sand with some preliminary investigation of fracking sand. The experimental data shows that the heat transfer coefficient should increase with sand velocity and should be on the order of 40 – 160 W/m^2-K.

3.2 Experimental Apparatus

Abdul-Aziz's experiment has been modified to study a different group of materials at higher flow rates. To facilitate the higher flow rates a new particulate lift system called the OLDS Elevator has been installed to provide for higher flow rates. In addition the reservoir above the heat exchanger, referred to as the constant head plenum, has been extended to help ensure flow symmetry. Finally, the higher flow rate causes a decrease in the temperature differential which will be compensated by increasing the input power into the heaters. The end result leads to a comparatively compact system as seen in Figure 1.

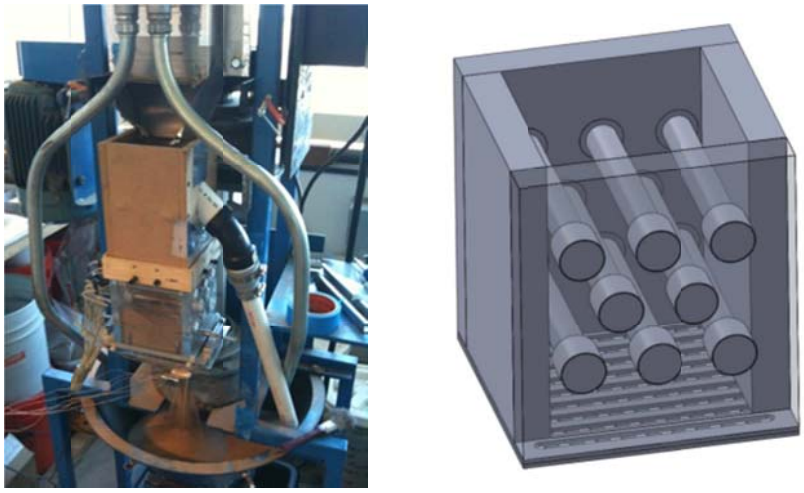

Figure 1: Left) OLDS Elevator and Heat Exchanger Apparatus
Right) Heat Exchanger Component

The OLDS Elevator is a device used to continuously move particulates in a vertical direction. The elevator uses a static auger with a rotating casing, the bottom of which sits inside a feed hopper filled with particulates. The rotation of the casing creates a shearing force on the particles that force the particles up static auger until they exit at the top of the elevator. These elevators use a variable frequency drive to control its operating speed. The apparatus that was used for this experiment is one of the first versions of the OLDS Elevator used frequently for demonstration purposes. As such several modifications are made to ensure steady operating conditions.

At the outlet of the elevator a constant head plenum is added. The plenum is used to create a constant head of particulates, ensure the heat exchanger is completely submerged, and provide a diverter for the particulates so that the flow rate is independent of the speed of the elevator. This is essential in order to prevent the experiment from overflowing. The constant head allow continuous operation under a saturated condition with similar flow patterns across all materials. The particulate flow speed through the heat exchanger is controlled at the heat exchanger outlet.

The heat exchanger box has inner dimensions of 0.114 m by 0.114 m by 0.114 m. The box is made up of four polymer walls and a steel bottom with the top left open. In this box eight cartridge heaters are placed in a staggered configuration.

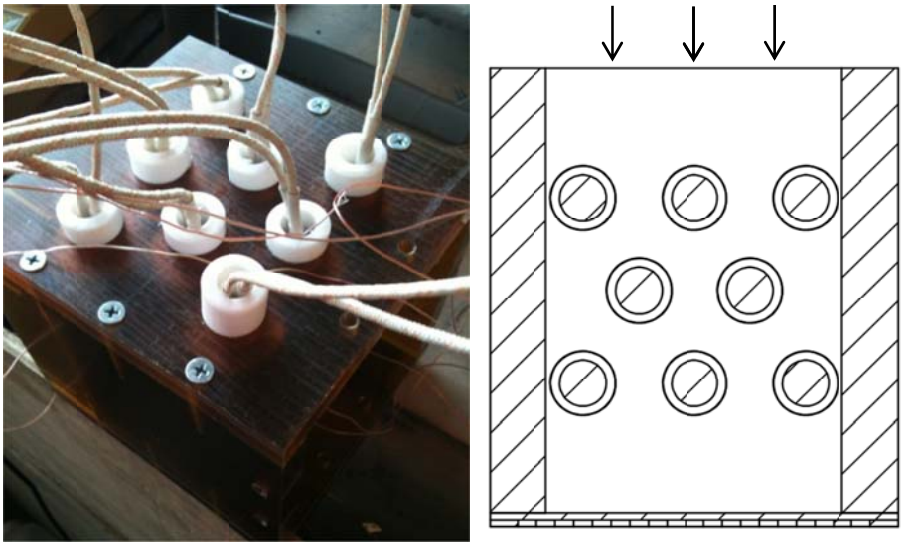

Figure 2: Heat Exchanger Section, Flow is in the Staggered Direction

This experiment tests the heat exchangers by heating the cartridges that replace the heat exchanger tubes which in turn heats the cold particulate flowing around the heaters. The first row contains 3 heaters, followed by two and then followed by another 3 heaters as shown in Figure 2. The cartridge heaters are electrically powered and act as a heat source for the system analogous to the hot pipes of a heat exchanger. Plastic end caps hold the heaters in position, half of the end caps are bored out to provide a path for the electrical wiring to travel.

Figure 3: 8 Cartridge Heaters Held in Position by End Cap

The nine heaters are wired in parallel with one another and are then connected in series with a watt meter followed by an autotransformer. These cartridge heaters are heaters incased in magnesium oxide with a stainless steel sheath. Each heater is 15.875 mm in diameter, 101.6mm in length and provide up to 200 Watts at 120 VAC (22). The autotransformer allows for testing at different power levels while the GPM 8212 Watt Meter is necessary due to the analog nature of the autotransformer (23). This pattern was chosen in order to simulate a section of the larger heat exchanger that will be used at Riyadh Tower Valley (RTV).

There are two variations of the heat exchanger due to the need to test both finned and un-finned tubing. Both variations utilize the same type of heater but the finned tube heat exchanger uses a finned tube sleeve which is inserted over the heat cartridges seen The finned tube have a 19.05 mm outer diameter, with a 1.65 mm wall thickness, a fin spacing of 2.4mm, with 8 fins per inch. The Heat Voss company created these finned tubes using carbon steel an example of which can be seen in Figure 4 (24).

Figure 4: Finned Tube

The bare tube heat exchanger design uses polycarbonate walls while the finned tube box is made out of a polymer known as amorphous thermoplastic polyetherimide (PEI) (25). PEI is a thermoplastic that was selected for the finned tubed test due to its higher operating temperatures. The higher operating temperatures are necessary due to the heat exchanger fins' proximity to the walls. In previous tests the finned design uses polycarbonate however the proximity of the fins to the walls causes the polycarbonate to soften.

Figure 5: Finned Tube Fusing with Polycarbonate and Sand Leading to Obstructions

This leads to the particulates fusing into the polycarbonate and causing an obstruction between the walls and the fins as shown in Figure 5. With prolonged exposure the plastic will melt eventually ruining the apparatus and contaminating the particulates. The properties of these two materials create a maximum temperature limit for this experiment of 100°C for the polycarbonate and 150°C for the PEI.

The bottom of the heat exchanger is composed of a series of three steel grates which forms the discharge system. Two grates are in a cross hatched pattern forming a single perforated plate. Without the cross hatched pattern bridging occurs when larger particle are used, (approximately the size of the Riyadh White Sand), which leads to disruptions in the flow over time. The third grate acts as a valve. Push screws are moved in order to move the discharge from a closed to completely open position. This valve is used to control the flow rate during an experiment. Bridging occurs when the gap between the grates is small enough that when several particulates attempt to move through the gap an obstruction is formed, lowering the overall flow rate. Bridging creates a transient decrease in the flow rate of the particulates and will eventually stop the majority of the flow through the heat exchanger. The stagnant portions of the flow lead

to a large buildup of heat that could potentially cause the heat exchanger to start melting. The second grate allows for a more uniform gap size that allows for testing of the Riyadh White Sand as shown in Figure 6.

Figure 6: Particle Discharge Using a Cross-Hatched Pattern

Despite these modifications bridging can still occur with the larger particles such as Atlanta Construction Sand and Play Sand which creates an upper limit as to the size of particulate that can be tested using this setup, as shown in Figure 7.

Figure 7: Evidence of Bridging Caused by Large Particulates

The outlet of the heat exchanger leads to a metal chute which completes the recirculation loop into the OLDS Elevator. The original purpose of the chute was to combine the discharge flow in order to observe an average outlet temperature and complete the recirculation loop.

Figure 8: Chute to Consolidate Exit Flow

To validate these results a control volume analysis is used to calculate the average outlet temperature. Temperatures have been recorded that violate energy conservation assuming uniform temperature as well as temperatures that are well below expected values. This discrepancy is due to the difficulties of obtaining a well-mixed particle temperature caused by temperature striations as seen in Brinn's paper. Due to the limited experimental height available, constrained by the lift height of the OLDs Elevator, a particulate mixer cannot be placed. As such the outlet temperature will be estimated using the energy balance. The discussion of the energy balance and values obtained for the outlet temperature can be seen in Chapter 6. Instrumentation of the apparatus is described in the next section.

3.3 Measurement and Instrumentation

The instrumentation for this experiment consists of temperature and mass flow measurements. The temperature was recorded at the inlet, outlet and surface of the heat exchanger. One E-type thermal probe was used inside the constant head plenum to measure the heat exchanger inlet temperature. This temperature is assumed to be uniform due to the mixing properties of the OLDS Elevator. The heat exchanger has surface thermal couples attached to the middle row of cartridge heaters. Each cartridge heater has three of these thermal couples attached to their surfaces. There is one on the top, one on the side and one the bottom. Symmetry of the cartridge heaters is assumed; as such the side thermocouple will have twice the weight when used for calculations.

Figure 9: Left) Left, Surface Thermocouple
Right) Right, Surface Thermocouple Placement for Bare Tubes

While the attachment of the thermocouples to the cartridge heaters is relatively simple the finned heaters are more delicate, the heaters have a fin spacing of 2.6 mm which is too small to use the same method as the bare tubes. Instead, a butane torch was used to preheat the fins, to

solder the thermocouples between the fins through capillary action. The surface thermocouples are attached at the base of the fins in the same relative locations as the non-finned heaters.

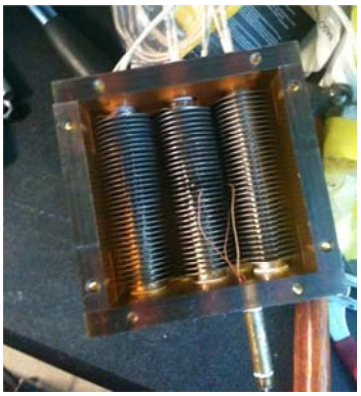

Figure 10: Finned Tube Placement in the Heat Exchanger Box

The three thermocouples on each heater are averaged in order to get a base temperature for the two instrumented heaters. Attempts to measure the outlet temperature have been made through the wire access pipe and at the outlet of the chute. The wire access pipe is positioned immediately after the heaters, and unfortunately does not allow for the particulates to mix. The lack of mixing results in unrealistic temperature readings. The second attempt places the thermocouple probe in the stream of the outlet chute; however the particulates entrain large amounts of air leading to lower than expected outlet temperature readings. The third attempt at measuring the outlet temperature after the chute employs a stainless steel screen mesh in to create a region where the thermal probe could be fully submerged to minimize air entrainment. While this sometimes provides accurate values, within 10% of predicted, this area is also frequently disturbed in order to measure the mass flow rate which ultimately leads to very inconsistent readings over the course of a test. Unfortunately, these options have proven unsuccessful as shown by a basic energy balance seen in Chapter 6. Several methods for mixing

particulate temperature have been considered but were not used due to the lack of sufficient vertical height within the apparatus. These methods can be seen in Appendix E. The thermocouples are monitored by a Model 34970 Agilent Data Acquisition Unit in order to record the data (26).

Figure 11: Attempts to Measure the Particulate Temperature

To measure the mass flow rate the 'bucket' test was used. A 500 mL beaker is used to measure the flow leaving the chute over a period of time tracked by a stop watch and a 500 ml beaker. Each measurement was taken three times at the beginning and end of each steady state period. Additionally, every thirty minutes throughout the experiment the mass flow rate was measured in order to ensure that the flow remained stable. This was essential in determining the presence of bridging and other obstructions.

In summary, the mass flow rate is measured using a beaker and stop watch. The temperature is measured by 6 K-type thermocouples are used to measure the surface temperature of the heaters and an E-type thermocouple measures the inlet temperature. These thermocouples are calibrated using a Platinum Resistance Thermometer.

3.4 Calibration

To ensure the accuracy of the instruments the thermocouples are calibrated using a Platinum Resistance Thermometer (PRT). The PRT has been calibrated by Burns Engineering to have an uncertainty of approximately ±0.0025 K. The thermocouples and PRT are placed into a water bath for calibration purposes (photos). The water bath is operated from 25 to 95°C. While this calibration applies to the majority of the majority of the results, some of the higher power settings cause the thermocouples to exceed the calibration. In the cases where the temperatures exceed the manual calibration, the Omega's manufacturer specifications are used instead. Typically the Omega uncertainty values are approximately ±2.2 K while the post calibration uncertainty is approximately ±0.004 K. The full calibration of the thermocouples can be seen in Appendix A.

3.5 Particle Material Selection and Properties

The materials selected are under consideration for use in a concentrating solar power tower plant. When considering a particulate the key factors to be aware of are its heat transfer coefficient, optical properties, particle size, and particle attrition. The optical properties are especially important due to the desire for high receiver efficiency. The particle size greatly influences the flow properties through the receiver, and particle attrition studies the change in the particles over time.

As a baseline test the first particulate chosen was fracking sand from Arizona Precision Sands. Fracking sand comes in a wide variety of sizes; however 70 mesh has been selected for use as a baseline material in this apparatus. In addition several other silica sands of various sizes were also studied such as Atlanta construction sand, Atlanta industrial sand, and Riyadh White Sand. Besides the silica sands, proppants were also observed. In comparison to sand, proppants

are made of alumina and are engineered to be a specific, spherical, size. This means that the proppants are much more uniform than the other materials.

Due to the non-uniform diameters of each batch of particles the particle size is defined by the Sauter Mean Diameter (SMD). The SMD represents a particles volume to surface area ratio as seen in the equation below where d_p is the diameter of the particle.

$$SMD = \frac{\text{Volume}}{\text{Surface Area}} = \frac{\frac{4}{3}\pi r^3}{4\pi r^2} = \frac{r}{3} = \frac{d_p}{6} \quad \textbf{3-1}$$

There are two primary methods to measure the SMD. One measures the size and shape of each individual particle using a microscope or other imaging device. The second uses a series of sieves to measure larger batches of material. The sieves allow for the particles to be measured within a certain diameter range based on the type of sieves used. Each sieve has a mesh that allows particles of a diameter below that of their size through, and stops any particles above that size.

For the use of meshes the following formula is used, assuming a constant density and spherical shape. Unfortunately, the sand particles that are used are not precisely spherical in shape however this is still the best method available to characterize the particle sizes.

$$SMD = \frac{1}{\sum \frac{w_i}{d_{p,i}}} \quad \textbf{3-2}$$

Table 3: Sauter Mean Diameter of the Materials Tested

	Fracking Sand	Atlanta Industrial Sand	Riyadh White Sand	Small Proppants	Large Proppants
Sauter Mean Diameter (mm)	0.229	0.301	0.343	0.268	0.758

The thermal properties of sand were measured using a KD2 Pro Thermal Properties Analyzer by Decagon Devices Inc., utilizing the TR-1 and SH-1 probes (12). The device was used to measure the bulk apparent thermal conductivity and the volumetric heat capacity as seen in Table 4. The bulk densities of the particulates were measured using a 500mL beaker, a graduated cylinder and a mass scale. Each of these particles also have a unique particle density which was not used in the analysis of the experiment. Instead, the bulk density is used due to it being more representative of plug flow.

Table 4: Summary of Measured Thermal Properties Using KD2-Pro

	Apparent Thermal Conductivity (W/m-K)	Volumetric Heat Capacity (MJ/m^3-K)	Density (kg/m^3)
Atlanta Industrial Sand	0.226	1.124	1364
Arizona Fracking Sand	0.250	1.232	1581
Construction Sand	0.224	1.178	1524
CarboHSP Proppant	0.263	1.839	2152
Accucast ID50-K	0.220	1.613	1823
Riyadh white sand	0.290	1.320	1561

The materials that are considered fall under two primary categories: silica sand and proppants. The sands that are tested consist of silica based sands with sizes varying from 1.34 mm to 0.21 mm. Proppants are small spherical beads made up of corundum and mullite (27). Proppants are most commonly used for the purposes of fracking but are considered a prominent

choice due to their specifically engineered size and dark coloring. The sizes of these proppants vary from 1.00 mm to 0.23 mm.

In addition to the materials in Table 4, construction sand was tested in the apparatus. The use of construction sand caused many difficulties in the experiment due to the non-uniformity in size. In particular, the construction sand contained particles which were larger than 595 microns. The larger particles allowed for bridging at the outlet of the heat exchanger leading to partial blockage of the outlet area.

Of the particulates studied, the sands are entirely silica based sand while the proppants are made from metal oxides. The chemical compositions are particularly important in studying various treatments to make the particles more absorptive as well as to try and estimate the specific heat of the particles.

3.5.1 Specific Heat Measurement

Measurements of the thermal properties for various particulates were taken using the KD2-Pro at room temperature. The KD2-Pro probe used is primarily used for liquids and solid blocks of materials. The interstitial space between the particulates causes large deviations from expected specific heat values using elemental composition.

To check the accuracy of the information the ID50-K has also been measured using a digital scanning calorimeter (DSC), the NETZSCH DSC 404C, from Clemson University. The results reaffirm that the specific heat found using the KD2-Pro are inaccurate.

For the purpose of this paper correlations have been created using elemental composition to calculate the specific heat of each material over a range of temperatures. The correlations are derived from the National Institute of Science and Technology (NIST) Heat Capacity data (28) (29) (30) (31). These values are given on a molar basis which is then converted to a mass basis

and divided by the bulk density values measured using a beaker. For the silica based sands the values are directly obtained from silica alpha quartz data. On the other hand the proppants are composed of several different elements.

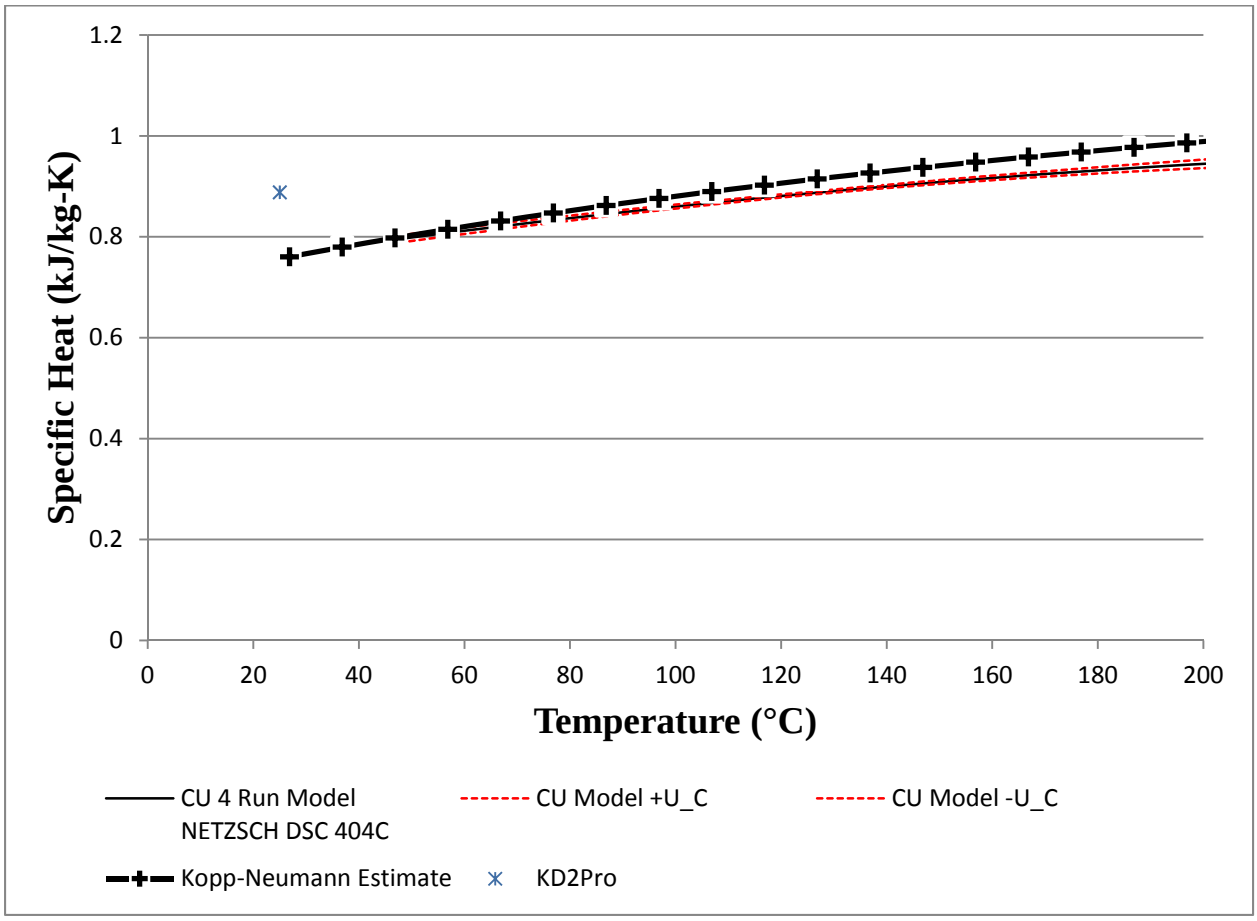

Figure 12: Comparison of KD2Pro Measurement Data
Against Kopp-Neumann Model and Empirical Data for ID50-K

As seen in Figure 12, the specific heat measured by the KD2Pro is significantly higher than expected. In comparison the specific heat measurements, made by Clemson University, at ~0.75 W/m^2-K over four repeated runs closely match the Koop-Neumann estimate at low temperatures. In addition, another DSC at Sandia National Labs was used to measure another

sample of the ID50-K. The results are significantly closer to the Koop-Neumann estimate than the KD2Pro. The other materials were also compared with the Koop-Neumann estimate and can be seen below.

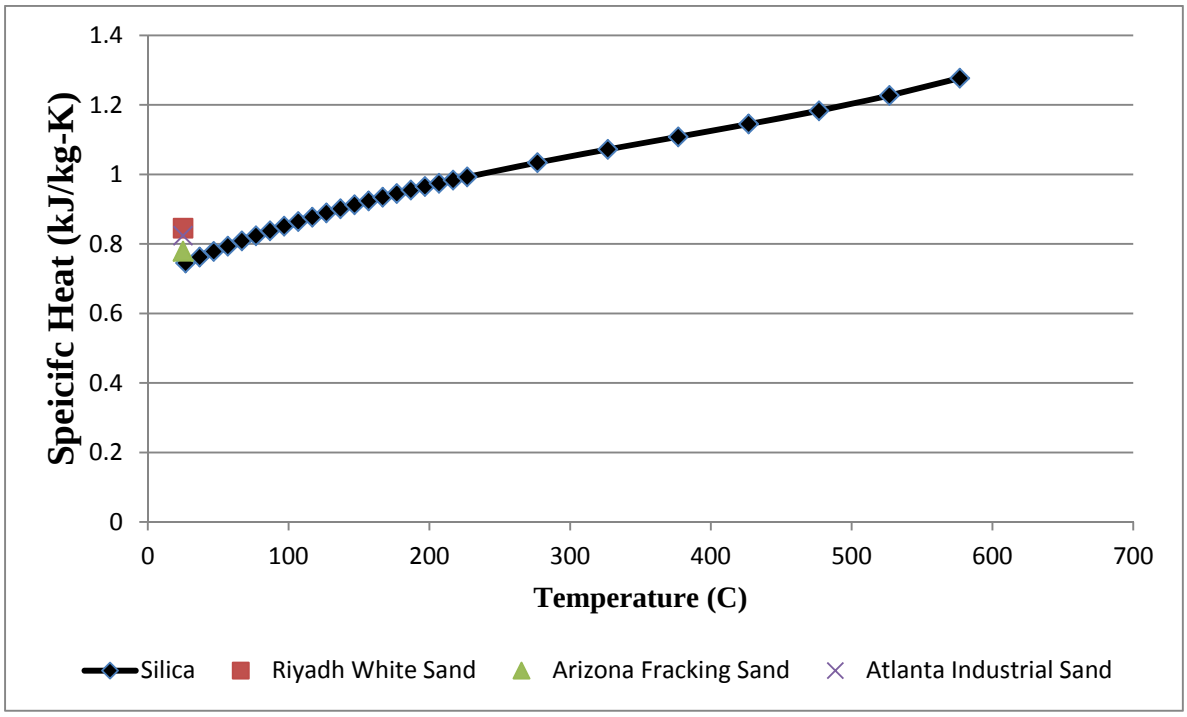

Figure 13: Comparison of KD2-Pro Measurement Data
Against Kopp-Neumann Model and Empirical Data for Silica Sands

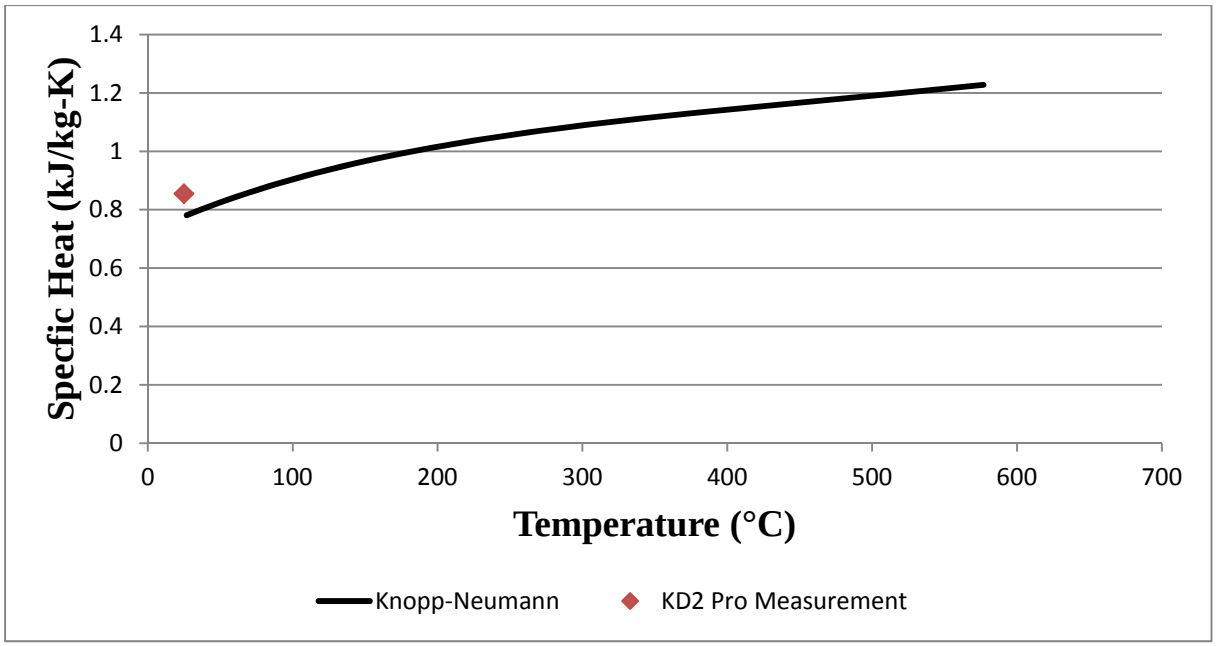

Figure 14: Comparison of KD2-Pro Measurement Data
Against Kopp-Neumann Model and Empirical Data for CarboHSP

With physical properties and thermal properties of these materials defined for this experiment attempts to create correlations between these various properties and the heat transfer coefficient of the particulates can be made. Additionally, the specific heat data is essential to calculating the outlet temperature from the heat exchanger. With this information the essential information that is needed to process the data has been researched and the experiment is conducted.

CHAPTER 4

EXPERIMENTAL METHODS

Prior to starting the experiment the type of heat exchanger must be chosen and inserted into the OLDS Elevator. The first step is to connect the constant head plenum with a series of clamps to the OLDS elevator. The clamps provide the structural support necessary for the rest of the system. The heat exchanger box is connected with screws to the constant head plenum and then sealed using aluminum tape. Once positioned, the diverter is then attached to the constant head plenum to prevent overflows. A level is then used to ensure that the apparatus is in a completely vertical orientation. Each of the heaters is then connected in parallel to the GPM 8212 Watt Meter which is connected to the autotransformer (23). Finally a chute is added to bottom of the heat exchanger to ensure the flow returns to the OLDS Elevator.

Once the apparatus is setup, approximately five gallons of a selected material is loaded into the OLDS Elevator. The critical factor in loading the OLDS Elevator is that the elevator does not run in a starved condition which can lead to pulses in the mass flow, or unsteady conditions. On the other hand overloading the OLDS Elevator will lead to the auger seizing. If seizing does occur a majority of batch must be emptied before another attempt can be made. While loading the particulate OLDS Elevator is also run at a slow speed in order to gradually fill the inner column.

After the Elevator is filled the grates at the bottom of the heat exchanger are adjusted using thumb screws. The screws are adjusted until the approximate flow speed desired is achieved. This flow speed is measured using a 500 mL beaker to catch the particulate flowing from the chute over a period of time measured by the stop watch. Care must be taken to observe that there

is still enough particulate in the Elevator that the temporary removal of this sample does not cause a starved condition to occur. This is especially significant at higher flow rates.

When the targeted flow rate has been achieved a sample is taken and sieved prior to beginning the test run. This measurement is taken three ties and is used to check for contamination and particle attrition. Particle attrition is measured both by the checking the density using a scale and a graduated cylinder as well as ensuring that the particle size distribution remains the same between runs.

With the apparatus in place and the particulate loaded the thermocouple probes are placed into the system. The inlet thermocouple is placed into the constant head plenum. The thermocouple is place in the center of the stream and measures a mixed particulate temperature due to the mixing that occurs within the OLDS Elevator. An outlet thermocouple is also placed at the discharge of the heat exchanger, but is ultimately irrelevant due to the difficulties in obtaining a mixed outlet temperature.

The autotransformer is then turned on and set to the approximately desired power level. The first setting is recorded but will drift by several Watts over the course of several hours and will be readjusted once a near steady state condition is achieved. As such the power is periodically recorded but only the steady state values are used. The experiment approaches steady state after several hours due to the large amount of thermal mass supplied by the OLDS Elevator. As the apparatus approaches steady state conditions the power and mass flow are once again measured. After thirty minutes of steady state operation the power and mass flow are measured before the power is shut off. The apparatus will continue to run in order to help cool the particulates prior to the next run.

CHAPTER 5

APPARATUS VALIDATION

To validate the experiment, the heat exchanger section of the experiment was removed and placed into a duct system. A blower is placed at the discharge of the system to pull air through the bare tubed heat exchanger assembly. By setting up the experiment with air as the thermal fluid the results can be compared to classical heat transfer literature for tubes and tube banks. As such, this experiment will measure the heat transfer coefficient of air and compare the results to correlations in the literature. To find the heat transfer coefficient the mass flow rate and inlet and outlet temperatures of the air as well as the surface temperatures of the tubes are measured.

5.1 Apparatus

The new setup is set up as a vertical column with a blower, located at region 1 in Figure 15, at the top to pull air through the system. The blower is a Rule 135 CFM blower and draws

power from a 120 Volt wall plug. An anemometer is used to verify that a constant flow rate of air

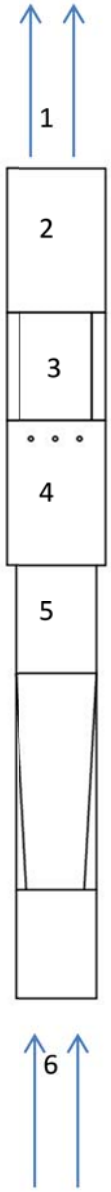

passes through the system at the holes in region 4 of

Figure 15. To measure the flow rate the device has a manually activated trigger for each measurement and will not be read directly into the DAQ unit. The anemometer has diameter of

110 mm round cross section which is then connected to the transition duct at region 6 of

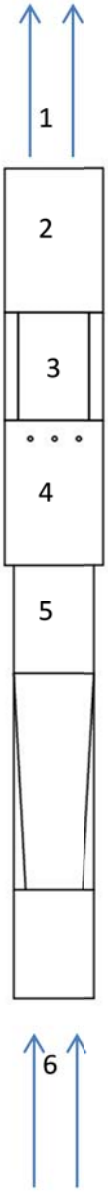

Figure **15**.

To transition between the anemometer and the heat exchanger system (region 3), a piece of sheet metal is shaped into a duct that starts as a 110 mm diameter round transitions to a 110 mm x 110 mm square cross section, region 5 of Figure 15.

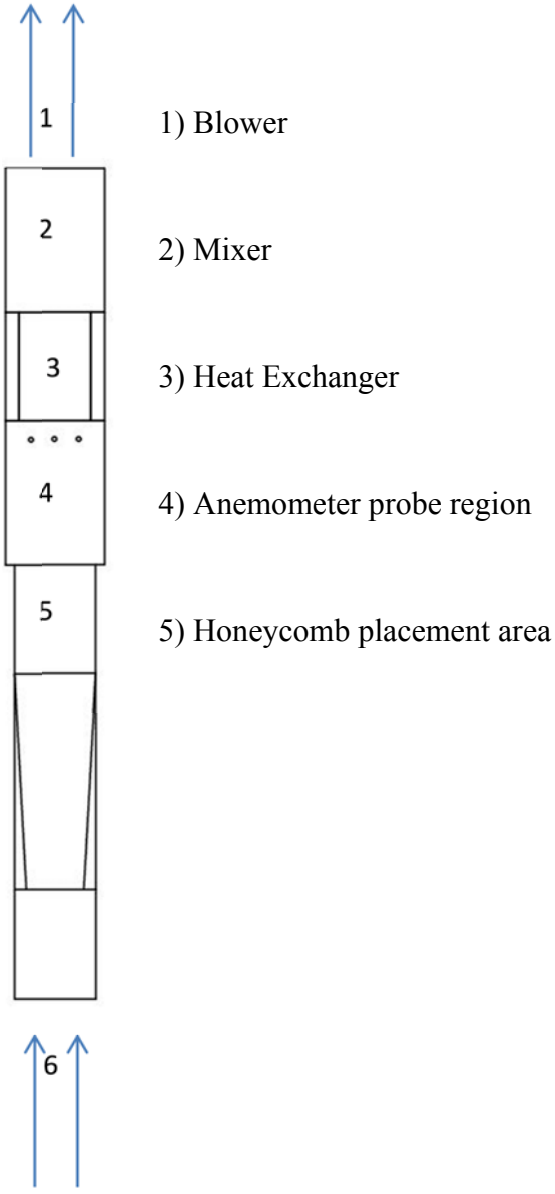

Figure 15: Air Validation Test Schematic

Preliminary experiments revealed that the air is pulled through a laminar fashion, such that a large boundary layer is present on the sides of the heat exchanger. To achieve a uniform flow an aluminum honeycomb panel (Figure 16) is placed at the exit of the transition region. Further details on achieving uniform flow can been in Appendix D.

Figure 16: Honeycomb Structure to Provide Uniform Air

Above the transition region is another 110 mm x 110 mm square duct which is used to measure inlet temperature and air speeds with an anemometer probe. There are three holes in the duct in which the probe is inserted into the air stream. This probe is used to verify that the airflow matches the anemometer at the inlet and has a fairly uniform air distribution.

To measure the inlet air temperature an Exposed Air RTD (P-L-1/10-1/4-6-0-P-3) calibrated to 1/10DIN accuracy (32) is inserted directly below the heat exchanger. A temperature gradient will form as the air flows through the heat exchanger, to measure the average outlet air temperature a series of metal plates are shaped to form an air mixer. The mixing section operates by forcing the air flows to converge at varying orientations prior to reaching another RTD to achieve a mixed outlet temperature.

This setup is used solely to validate that the apparatus operates as expected. For the sake of making an easily comparable system the heat exchanger section will use the bare tubed configuration instead of the finned configuration. Heat transfer data from this experiment will be compared to classic heat transfer literature.

5.2 Experimental Methods

Once the apparatus is in position the blower is connected to a 12 volt power source which is in turn plugged into a standard wall socket to provide power. The Airflow LCA 30VT anemometer is used to check the flow speed several times and ensure a constant air speed is achieved (33). After the flow is steady, the powers to the heaters are turned on and adjusted using an autotransformer. A GPM 8212 Watt Meter is used to measure the power, voltage and current supplied by the autotransformer. The power tends to drift as the heaters increase in temperature. As such there is an initial period of time during which the power is repeatedly adjusted to achieve a power setting of ~150 Watts. After the steady state period is reached, the watt meter and anemometer data is frequently recorded.

To observe the effects of heat loss through the wires in the experiment the wires were wrapped in pipe insulation and the heat exchanger unit wrapped with insulation wool. Once insulated, experiment was repeated in order to calculate the heat transfer coefficient and see if the results differed between insulated and non-insulated tests.

5.3 Data Processing

The calculations used to find heat transfer coefficient of air closely matches the found in Chapter 4. Firstly the surface area of an individual bare tube is calculated using equation 5-1.

$$A_{bare} = 2\pi r_1 L \qquad \textbf{5-1}$$

Then the log mean temperature difference (LMTD) is calculated. $T_{base,top}$ and $T_{base,bot}$ represent the average value of the thermocouples that are placed on the top and bottom heaters respectively. Of the thermocouples placed on the heaters, the side thermocouples are double weighted due to

an assumption of symmetry. Important to note, is that the flow is reversed in the air validation experiment. As such the bottom heater is actually upstream of the top heater.

$$LMTD = \frac{(T_{\text{heater,up}} - T_{\text{air,in}}) + (T_{\text{heater,down}} - T_{\text{air,out}})}{\ln\left(\frac{T_{\text{heater,up}} - T_{\text{air,in}}}{T_{\text{heater,down}} - T_{\text{air,out}}}\right)} \quad \textbf{5-2}$$

With the *LMTD* calculated the heat transfer coefficient is found by dividing the power input by the surface area of the heater and the *LMTD*.

$$h_{\text{air}} = \frac{\dot{Q}_{\text{tube}}}{A_{\text{bare}} LMTD} \quad \textbf{5-3}$$

Of important note, this is an indirect calculation for the heat transfer of the heat exchanger, instead the value calculated is for the heat transfer from the surface of the heat exchanger to the air.

For validation purposes a number of correlations have been researched for heat transfer on similar geometries. Table 5 shows the correlations used for heat transfer over a single tube and includes a variety of empirical data.

Table 5: Heat Transfer for Single Tube Correlations

Source	Correlation
Hilpert	$Nu_D = \frac{\bar{h}D}{k} = C_h \, \mathrm{Re}_D^m \, \mathrm{Pr}^{1/3}$
ASHRAE	$Nu_D = \frac{\bar{h}D}{k} = 0.24\left(\frac{\mathrm{G\ D_o}}{\mu}\right)^{0.6^{1/3}}$
Churchill	$Nu_D = \frac{\bar{h}D}{k} = .0.3 + \frac{.62\sqrt{\mathrm{Re}}\mathrm{Pr}^{1/3}}{(1+(.4/\mathrm{Pr})^{2/3})^{1/4}}\left(1+\left(\frac{\mathrm{Re}}{282000}\right)^{5/8}\right)^{4/5}$
Zhukauskas	$Nu_D = \frac{\bar{h}D}{k} = 0.51\sqrt{\mathrm{Re}}\mathrm{Pr}^{0.37}\left(\frac{\mathrm{Pr}}{\mathrm{Pr_s}}\right)^{1/4}$

Table 6 lists the correlations for the heat transfer of air over a tube bank. The constants in the correlations refer to a table of parameters based on the staggering and spacing of the individual tubes.

Table 6: Heat Transfer for Tube Bank Correlations

Source	Correlation
Colburn	$Nu_D = \frac{\bar{h}D}{k} = 0.33\left(\frac{G_{max}D_o}{\mu}\right)^{0.6}\left(\frac{\mu c_p}{k}\right)^{1/3}$
Zhukauskas	$Nu_D = \frac{\bar{h}D}{k} = C_{z2}\,C_z Re_{D,Max}{}^m Pr^{0.36}\left(\frac{Pr}{Pr_s}\right)^{1/4}$
Grimison	$Nu_D = \frac{\bar{h}D}{k} = 1.13C_g Re_{D,max} Pr^{1/3}$

5.4 Uncertainty Analysis

The uncertainty analysis for the validation experiment will be similar to that of the actual experiment with many of the same components in use. The heat exchanger unit has been measured using a caliper with an accuracy of ±0.001. Each of the thermocouples attached to the heaters in the bare tubed unit has a layer of temperature resistant Kapton, a polyimide film, tape surrounding the thermocouple bead to hold it in position. The thermocouples are each calibrated using a PRT calibrated by Burns Engineering (34). Further details can be seen in Appendix A. This calibration leads to each surface thermocouple having an uncertainty of approximately ±0.004 K. The inlet and outlet thermocouples air resistance temperature detectors (RTD) were purchased from Omega with a ±1/10DIN (±0.00425°C) accuracy (32). The table below shows the calculation of heat transfer coefficient for air flowing through the bare tubed heat exchanger.

Table 7: Uncertainty Table for the Calculation of the Heat Transfer Coefficient of Air Through the Bare Tubed Heat Exchanger

Measurement	U_{xi}	Influence Coefficient, $\frac{\partial \dot{m}}{\partial x_i}$	$U_i^2 = \left(U_{xi}\frac{\partial h}{\partial x_i}\right)^2$ $(W/m^2\text{-}K)^2$	$\frac{U_i^2}{U_B^2}$ (%)	Basis	Source
Diameter of Tube	0.001 m	85.24	7.3E-03	6.05	Caliper Measurement	
Heat Input to One Tube, Q	0.6096 W	0.55	1.1E-01	92.73	Assumed	
Heater Length, L	0.001 m	13.32	1.80E-04	0.15	Caliper Measurement	
TC 1, Top Tube, Top	0.0039 K	0.15	3.42E-07	0.00	Calibration	
TC 2, Top Tube, Side	0.004 K	0.32	1.64E-06	0.00	Calibration	
TC 3, Top Tube, Bottom	0.0057 K	0.16	8.32E-07	0.00	Calibration	
TC 4, Bottom Tube, Top	0.004 K	0.14	2.99E-07	0.00	Calibration	
TC 5, Bottom Tube, Side	0.0049 K	0.26	1.67E-06	0.00	Calibration	
TC 6, Bottom Tube, Bottom	0.0039 K	0.14	2.85E-07	0.00	Calibration	
Inlet TC	0.00425 K	0.55	5.41E-06	0.45	Manufacturing Standards	(1)
Outlet TC	0.00425 K	0.64	7.40E-06	0.62	Manufacturing Standards	(1)
		sum of U_i^2 =	0.12	100		
		Expanded Uncertainty U_B=	0.34 W/m^2-K			

(1) Referencing Omega RTD standards (32)

5.5 Results

Table 8: Heat Transfer Coefficient for Experimental Data

	Heat Exchanger	Upstream Heater	Downstream Heater
Insulated Run 1	52.945 ± 0.344	57.284 ± 0.370	48.826 ± 0.320
Insulated Run 2	52.053 ± 0.083	57.517 ± 0.091	47.024 ± 0.079
Insulated Run 3	51.984 ± 0.340	57.447 ± 0.370	46.955 ± 0.307
Non Insulated Run 1	53.247 ± 0.350	57.515 ± 0.380	49.190 ± 0.320
Non Insulated Run 2	52.020 ± 0.340	57.528 ± 0.370	46.960 ± 0.300
Non Insulated Run 3	53.366 ± 0.350	57.894 ± 0.380	49.081 ± 0.320

Table 9: Heat Transfer Coefficient from Literature for Single Tube Models

	ASHRAE	Newton's Law of Cooling	Hilpert	Churchill	Zhukauskas
Insulated Run 1	56.97 ± 0.35	57.57 ± 0.38	47.81 ± 0.23	54.02 ± 0.29	46.99 ± 0.24
Insulated Run 2	56.65 ± 0.20	56.03 ± 0.13	47.65 ± 0.13	53.77 ± 0.17	46.80 ± 0.14
Insulated Run 3	57.38 ± 0.35	55.98 ± 0.36	48.09 ± 0.23	54.37 ± 0.29	47.28 ± 0.24
Non Insulated Run 1	56.37 ± 0.34	58.22 ± 0.38	47.44 ± 0.23	53.53 ± 0.29	46.59 ± 0.24
Non Insulated Run 2	57.50 ± 0.35	55.98 ± 0.36	48.19 ± 0.23	54.48 ± 0.29	47.38 ± 0.24
Non Insulated Run 3	57.05 ± 0.35	57.73 ± 0.38	47.86 ± 0.23	54.09 ± 0.29	47.05 ± 0.24

Table 10: Heat Transfer Coefficient from Literature for Tube Bank Models

	Colburn	Zhukauskas	Grimison, 10 Row	Grimison, 3 Row
Insulated Run 1	97.41 ± 0.60	89.55 ± 0.55	109.14 ± 0.62	90.63 ± 0.52
Insulated Run 2	96.83 ± 0.34	89.02 ± 0.31	108.60 ± 0.36	90.17 ± 0.30
Insulated Run 3	98.09 ± 0.60	90.18 ± 0.55	109.89 ± 0.62	91.25 ± 0.52
Non Insulated Run 1	96.37 ± 0.59	88.59 ± 0.54	108.07 ± 0.61	89.74 ± 0.51
Non Insulated Run 2	98.30 ± 0.60	90.36 ± 0.55	110.13 ± 0.63	91.45 ± 0.52
Non Insulated Run 3	97.55 ± 0.59	89.68 ± 0.55	109.66 ± 0.62	91.05 ± 0.52

5.6 Discussion

As seen from the table in the results section, the heat transfer coefficient of air from these tests closely matches the expected results from heat transfer models for a single tube. The

theoretical correlations for a single tube ranged from ~48-58W/m^2-K, while the tube bundle ranged from ~90-98W/m^2-K.

The heat transfer coefficient for the full bundle is approximately 53 W/m^2-K. This was calculated using the LMTD of the bundle and the central surfaces. To confirm this, the single tube heat transfer coefficient was calculated as well. For the central tube in the first row that is impinged by the incoming air, the heat transfer coefficient is ~47 W/m^2-K. This closely matches the literature values calculated by Hilpert. Further literature review shows that this value is also within 20% of the expected ASHRAE values as found by Churchill. The measured tube in the third row has a heat transfer coefficient of ~57 W/m^2-K; the value is well within expected values for the *h* of a single tube and is higher than the upstream tube as expected due to the additional turbulence from the prior row.

In comparison to the heat transfer coefficients expected from a tube bank, the experimental values were much lower. This does not come as a surprise since the tube bank was not tested in the turbulent conditions expected by these correlations. In addition, the heat exchanger only has three rows in comparison to the typically expected 10 or more rows which increase the turbulence and heat transfer coefficient even further. The size of the heat exchanger is also significantly smaller than those typically used and the wall effects reduce the turbulence of the heat exchanger even further leading to the difference between the experimental and theoretical tube bank values.

The experiment was also conducted at heater surface temperatures that closely matched those in the particulate experiment. As can be seen above the heat loss through the wires during the non-insulated runs are negligible; as evidenced by the similar heat transfer coefficients obtained in the insulated runs.

5.7 Conclusion

In comparison, expected values for heat transfer of air over a tube bundle are ~95 W/m^2-K. As such the geometry of this lab scale heat exchanger better approximate that of a series of individual tubes in comparison to a tube bundle. Nevertheless, the experiment verifies the apparatus by achieving heat transfer coefficients near that of the literature.

CHAPTER 6

DATA PROCESSING

With the previous results validating the experimental apparatus the data from the particulate experiments can be confidently analyzed. This section will cover the analysis of both the finned and bare tube heat exchanger. The primary goal of which is to calculate the heat transfer from the surface of the heat exchanger to the particulate flow. As such this is not a direct calculation of the heat transfer of the heat exchanger but instead a calculation of the heat transfer coefficient of the particulates analogous to the convection of fluids. Additionally, the uncertainty analysis will also be described.

6.1 Bare Tubed Heat Exchanger

To conduct the heat transfer analysis the geometry of the heat exchangers with particulates is first calculated using a simple calculation to find the surface area of the a single bare tubed cartridge heater as seen in equation 6-1.

$$A_{\text{bare}} = 2\pi r_1 L \qquad \textbf{6-1}$$

In order to calculate the average heat transfer coefficient across a bundle of tubes, the logarithmic mean temperature difference (LMTD) between the tube surface temperature and the particulate bulk temperature is calculated using equation 6-2.

$$\text{LMTD} = \frac{(\text{T}_{\text{base,top}} - T_{\text{par,inet}}) + (\text{T}_{\text{base,bot}} - T_{\text{par,outlet}})}{\ln\left(\frac{\text{T}_{\text{base,top}} - T_{\text{par,inet}}}{\text{T}_{\text{base,bot}} - T_{\text{par,outlet}}}\right)} \qquad \textbf{6-2}$$

The $T_{\text{base,top}}$ and $T_{\text{base,bot}}$ are the average temperatures of the measured cartridge heaters. The thermocouples are averaged with the side thermocouple having a twice the weight of the bottom

and top thermocouples. This method of calculating the average temperature was made under the assumption of the heaters having a symmetrical temperature profile.

As previously mentioned, an accurate outlet temperature could not be measured due to the difficulties in finding a mixed outlet flow temperature. To compensate for this a control volume analysis is performed. The analysis is performed by assuming a conduction model where the highest temperature is in the center of the heat exchanger. The heat is then conducted through stagnant sand followed by the walls of the heat exchanger and energy is finally released into the stagnant ambient air. Though this heat loss is essentially negligible it will be included for completeness.

The thermal properties of the model are found using the thermal conductivities of sand, the wall material (PEI or Polycarbonate) and the heat transfer coefficient of stagnant air at the average particle temperature.

$$T_{\text{par,avg}} = \frac{T_{\text{par,inlet}} + T_{\text{par,outlet}}}{2} \quad \textbf{6-3}$$

This material data is then used to compute the *R* values which is then used to find the overall *UA* of the heat exchanger.

$$U = \frac{1}{R_{\text{wall}} + R_{\text{part}} + R_{\text{air}}} \quad \textbf{6-4}$$

With the *UA* found a simultaneous equation solver, Engineering Equation Solver (EES) is used to simultaneously calculate the heat loss and the particle outlet temperature using equations 6 and

$$UA_{\text{surface,box}} = \frac{\dot{Q}_{\text{loss}}}{T_{\text{par,avg}} - T_{\text{amb}}} \quad \textbf{6-5}$$

The UA value for the box is 0.24 W/K which is used to implicitly find the heat loss and the outlet temperature. With such a low *UA* value the heat exchanger loses approximately six watts

of heat which is insignificant to the upwards of five hundred watts that the heaters are generating.

$$\dot{Q}_{loss} = (UA_{\text{surface, box}})(T_{\text{par, avg}} - T_{\text{amb}}) \quad \textbf{6-6}$$

$$T_{\text{par,out}} = T_{\text{par,in}} + \frac{\dot{Q} - \dot{Q}_{loss}}{\dot{m}c_{\text{p}}} \quad \textbf{6-7}$$

The average heat transfer coefficient is calculated in equation 8, which represents the average heat transfer coefficient over the entire finned surface of the tube bundle. h_{average} is based on *LMTD* (equation 6-8) between the surface temperature at the base of the fins and the sand bulk temperature.

$$h_{\text{average}} = \frac{\dot{Q}_{\text{tube}}}{A_{\text{bare}} LMTD} \quad \textbf{6-8}$$

6.2 Finned Tube Heat Exchanger

The geometry of the finned heaters is calculated using equations 6-9 through 6-12. These equations calculate the surface area of a finned tube heat cartridge. The first equation finds the area of the base of the finned tube.

$$A_{\text{base}} = 2\pi r_1 (L - tN_{\text{fins}}) \quad \textbf{6-9}$$

To find the Area of a fin the following equation is used.

$$A_{\text{fin}} = 2\pi (r_{2c}^2 - r_1^2) \quad \textbf{6-10}$$

The r_{2c} value calculated is a corrected radius value used in calculating the fin efficiency.

$$r_{2c} = r_2 + \frac{t}{2} \quad \textbf{6-11}$$

The total surface area of a finned tube can be found by summing the base area with the area of the fin multiplied by the number of fins.

$$A_{\text{fin,tube}} = A_{\text{base}} + A_{\text{fin}} N_{\text{fins}} \quad \textbf{6-12}$$

Similar to the bare tube case, equation 6-2 is used to calculate the LMTD for the finned tube case. To calculate the outlet temperature equations 6-3 through 6-7 are used with a *UA* value of 0.2934 W/K. The difference the UA value is due the use of PEI rather than polycarbonate as the material of the heat exchanger wall.

For the finned tube heat exchanger the following heat transfer formula is used to calculate the effective heat transfer coefficient and the fin efficiency.

$$\dot{Q}_{\text{tube}} = h_{\text{effective}} A_{\text{base}} LMTD + h_{\text{effective}} A_{\text{fin}} LMTD \, \eta_{\text{fin}} N_{\text{fins}} \quad \textbf{6-13}$$

Similar to h_{average} for the bare tube heat exchanger, $h_{\text{effective}}$ term represents the effective heat transfer coefficient over the entire finned surface of the finned tube bundle. The LMTD value calculated is the same as equation 6-2 for the bare tube bundle.

$$c_{\text{fin}} = \frac{2r_1}{m(r_2^2 - r_1^2)} \frac{K_1(mr_1)I_1(mr_{2c}) - I_1(mr_1)K_1(mr_{2c})}{I_0(mr_1)K_1(mr_1) - K_0(mr_1)I_1(mr_{2c})} \quad \textbf{6-14}$$

$$m = \sqrt{\frac{2h_{\text{effective}}}{k_{fin} t}} \quad \textbf{6-15}$$

η_{fin} is the fin efficiency and represents the ratio between heat transfer rate from the fin and that from an identical fin with an infinite thermal conductivity. The fin efficiency was found using the above analytical solution (35). In equation 6-14 I_i and K_i respectively represent the i-th order Bessel Function of the first and second kind. For the variable *m, k* is the thermal conductivity of the material and *t* is the thickness of the fins.

$$h_{\text{apparent}} = \frac{\dot{Q}_{\text{tube}}}{A_{bare} LMTD} \quad \textbf{6-16}$$

The previous equation uses the same q from the finned heat exchanger experiment in order to calculate the h_{apparent} which represents the heat transfer coefficient that would be required for a bare tube bundle to transfer the same heat rate for the same $LMTD$ value as the finned tube. This

ratio is primarily used to quantify the advantage of the finned heat exchanger in comparison to the bared tubed heat exchanger in terms of heat.

$$\in_{\text{fin}} = \frac{h_{effective}}{h_{average}} \qquad \textbf{6-17}$$

Equation 6-17 shows the fin effectiveness which is the enhancement ratio between the heat transfer rate with the fin and the heat transfer rate without the fin for the same surface temperature. A minimum value of two is usually required for the fin geometry to be considered effective.

6.3 Uncertainty Analysis

The uncertainty is calculated for each heat transfer coefficient. This section will present the most significant sources of uncertainty and how each is addressed. In addition to the systematic uncertainty (U_b), or bias, the statistical uncertainty of the experiment will also be addressed.

$$h_{\text{air}} = \frac{\dot{Q}_{\text{tube}}}{A_{\text{bare}} LMTD} \qquad \textbf{5-3}$$

Equation 6-16 is the main focus of these derivations. The heat from the tube is determined by the power input as measured by a GPM 8212 watt meter. The device has an error of ±1.8W when used in the 600 W range which was chosen as the uncertainty for all the lower power measurements as well in order to be conservative. The watt meter is connected in series with an autotransformer and the heat exchanger unit. In the bare tube heat exchanger calculations this is the second most significant variable in comparison this becomes the most significant variable for the finned tube calculations. For the finned tube calculation the most significant factor is the specific heat uncertainty of 10%. The uncertainty of the specific heat has a major influence since it is used to predict the outlet temperature in Equation 6-7.

$$T_{\text{par,out}} = T_{\text{par,in}} + \frac{\dot{Q} - \dot{Q}_{loss}}{\dot{m} c_{\text{p}}} \qquad \textbf{6-7}$$

Another significant factor is the thermal conductivity used in the finned tubes due to a conservative upper estimate of 10% uncertainty. In reference to the literature by Leitner, at the temperature ranges that this experiment operates in a 3% is expected. This source of error is considered when calculating the heat transfer coefficient in combination with the fin efficiency.

The ordered thermocouples originally have an uncertainty of ±2.2 K according to Omega's manufacturing standards (36). To minimize this major source of error, a Platinum Resistance Thermometer (PRT) probe calibrated by Burns Engineering is used to reduce the resulting error due to temperature measurements.

The majority of the thermocouples have been calibrated to approximately ±0.004 K with the exception of the bottom thermocouple for the top finned tube. The thermocouples were previously attached to the fins from the previous experiment and as such were not removed. Instead the fins and cartridge heaters with the attached thermocouples are inserted into a water bath. Originally the calibration was attempted using a fluidized bath; more details can be seen in Appendix B. Unfortunately this attempt led to the destruction of one of the original thermocouples; instead the manufacturer's uncertainty is used. For the other thermocouples a water bath was used despite the limited temperature range.

The calibration above shows a reliable linear correlation between the temperature of the thermocouples and the calibration standard. The calibration method involved taking a large number of data points such that the statistical uncertainty was minimized to an almost negligible value. As such the combined uncertainty was close to the value of the bias in the PRT.

Table 11: Expanded Uncertainty for the Heat Transfer Coefficient of Finned Tubes - Example for Riyadh White Sand at ~10mm/s and 891 W

Measurement	U_{xi}	Influence Coefficient, $\frac{\partial \dot{m}}{\partial x_i}$	$U_i^2 = \left(U_{xi}\frac{\partial h}{\partial x_i}\right)^2$ $(g/m^2\text{-}s)^2$	$\frac{U_i^2}{U_B^2}$ (%)	Basis
Diameter of Tube	0.001 m	-157.50	2.48E-02	0.04	Caliper Measurement
Thermal conductivity of finds, k	5.192 W/m-K	0.90	2.19E+01	34.59	Assumed
Heater Length, L	0.001 m	-255.90	6.55E-02	0.10	Caliper Measurement
Heat Input, Q	1.8 W	0.27	2.43E-01	0.38	Calibration
Mass	0.0001 kg	-19.74	3.90E-06	0.00	Calibration
Time	0.01 s	2.33	5.42E-04	0.00	Instrument
TC 1, Top Tube, Top	0.0030 K	1.69	2.56E-05	0.00	Calibration
TC 2, Top Tube, Side	0.0030 K	1.68	2.55E-05	0.00	Calibration
TC 3, Top Tube, Bottom	2.2 K	1.68	13.70925	21.60	Manufacturing Standards
TC 4, Bottom Tube, Top	0.0032 K	2.00	4.08E-05	0.00	Calibration
TC 5, Bottom Tube, Side	0.0033 K	2.00	4.34E-05	0.00	Calibration
TC 6, Bottom Tube, Bottom	0.0028 K	2.00	3.13E-05	0.00	Calibration
TC 7, Inlet	0.0074 K	10.93	6.54E-03	0.00	Calibration
Specific Heat	0.024 kJ/kg-K	52.37	1.579747	43.23	Upper Estimate
TC 8, Ambient	5 K	0.01	5.18E-03	0.00	Upper Estimate
Fin thickness	0.000001 m	-10200.00	1.04E-02	0.02	Caliper Measurement
Wall Thermal Conductivity	0.2425 W/m-K	3.44	6.96E-01	0.01	Manufacturer
		sum of U_i^2 =	38.04		
		Expanded Uncertainty U_B=	6.17 W/m^2-K		

The uncertainty results, seen in Table 11, are from the calculation of the U_B of the heat transfer coefficient similar to that used by Kline (37). For brevity, the table omits repeated

measurement values that are used for the mass and time as well as any variables that have no significant relevance. Example results for the bare tubed experiment can be seen in the Appendix B.

While the table above calculates the U_B, the value only applies for a single data point during the chosen steady state period. To include the statistical uncertainty, each of the individual data points has the heat transfer coefficient value and its uncertainty calculated. Then each of those values are averaged over the steady state period. For the example used in the table above 126 heat transfer coefficient values and their uncertainties are averaged to find a value of 142 W/m^2-K with an average of U_B ±6.57and U_A of ±0.79. This leads to a combined uncertainty of ±6.62.

CHAPTER 7

RESULTS

The bare tube heat exchanger configuration is used as a baseline of comparison for the finned heat exchanger configuration.

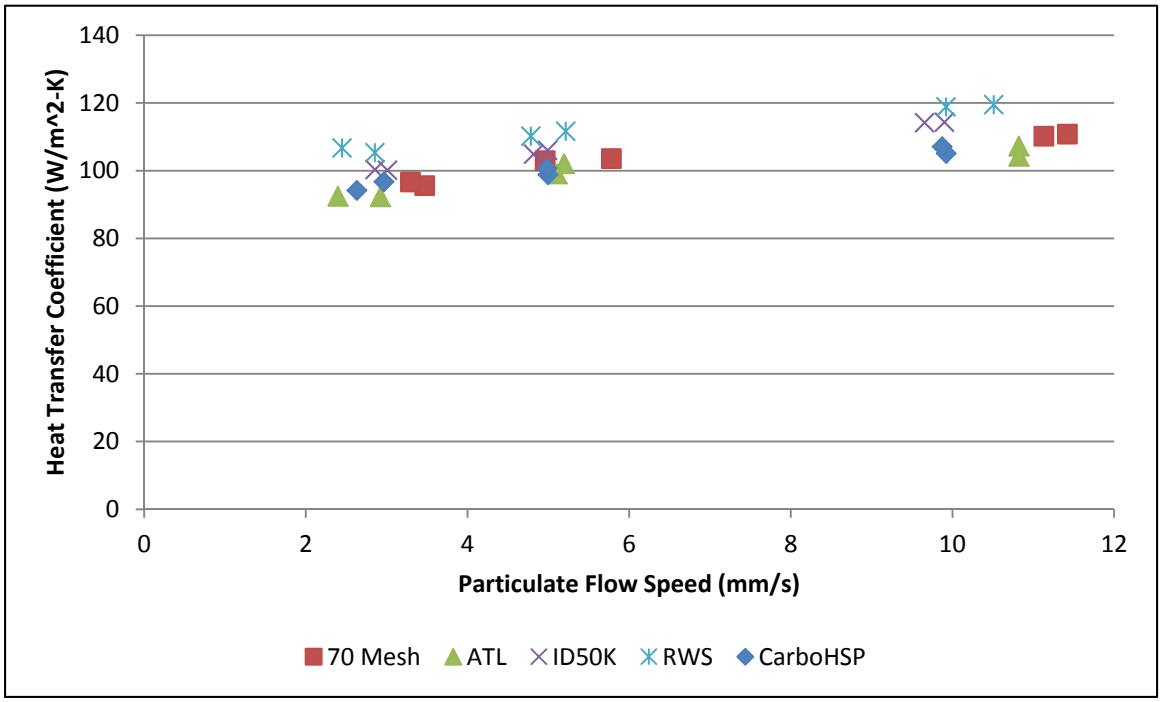

Figure 17: Heat Transfer Coefficient for Bare Tube Heat Exchanger

The Riyadh White Sand (RWS) and the ID50-K has the highest heat transfer coefficient and shows the most potential for use in a bare tubed heat exchanger. One important factor to note is that the Sauter Mean Diameter shows no direct correlation to the heat transfer coefficient. The most likely cause of this is that though the average diameter has been calculated, the smaller particulates fill in gaps within the particulate flow allowing for better contact with the heat exchanger. However, this may change if a mono-dispersed material is tested.

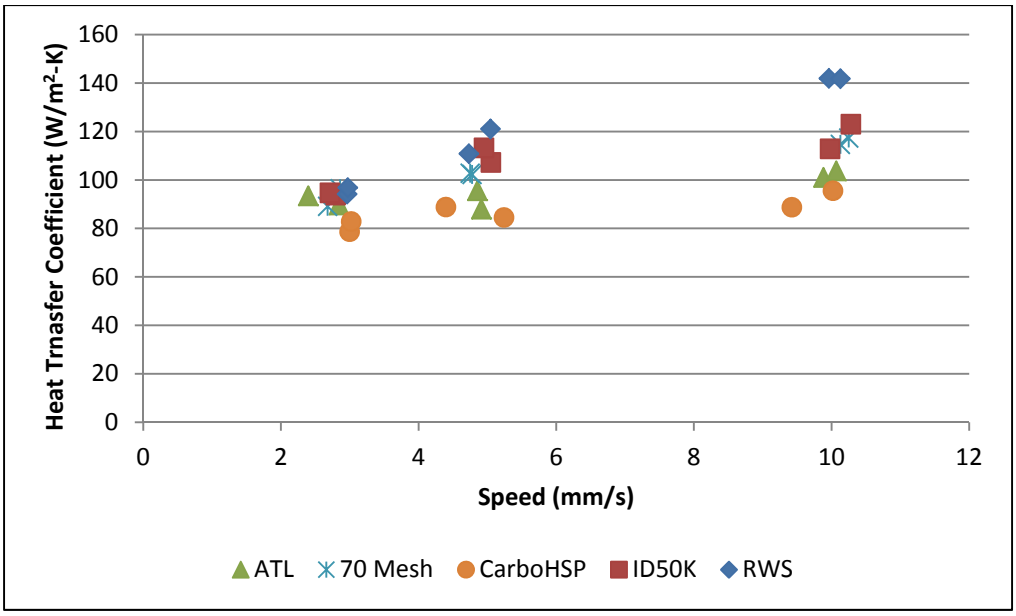

Figure 18: Effective Heat Transfer Coefficient of Particulates in a Finned Tube Heat Exchanger Configuration

Similar to the bare tubed heat transfer coefficient, the particulate side heat transfer coefficient is higher for the RWS and the ID50-K. These values take into account the additional area that fins provide, but are overall higher than the $h_{effective}$ of the bare tubes. This is most likely due to the shape of the fins forcing the particulates into contact with the heat exchanger during a plug flow regime.

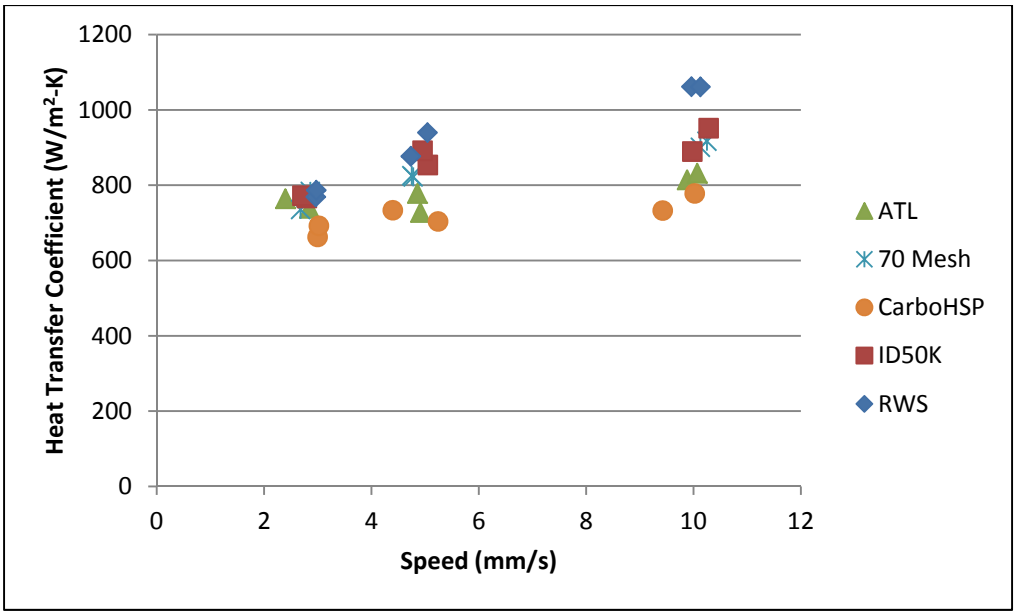

Figure 19: Apparent Heat Transfer Coefficient of Finned Tube Heat Exchanger Configuration

To compare the finned configuration to the bare tubed configuration the heat transfer coefficient is calculated using the bare tube geometry but with the data obtained from the finned configuration. The data above shows that the fins provide nearly an order of magnitude more heat transfer in comparison to the bare tube.

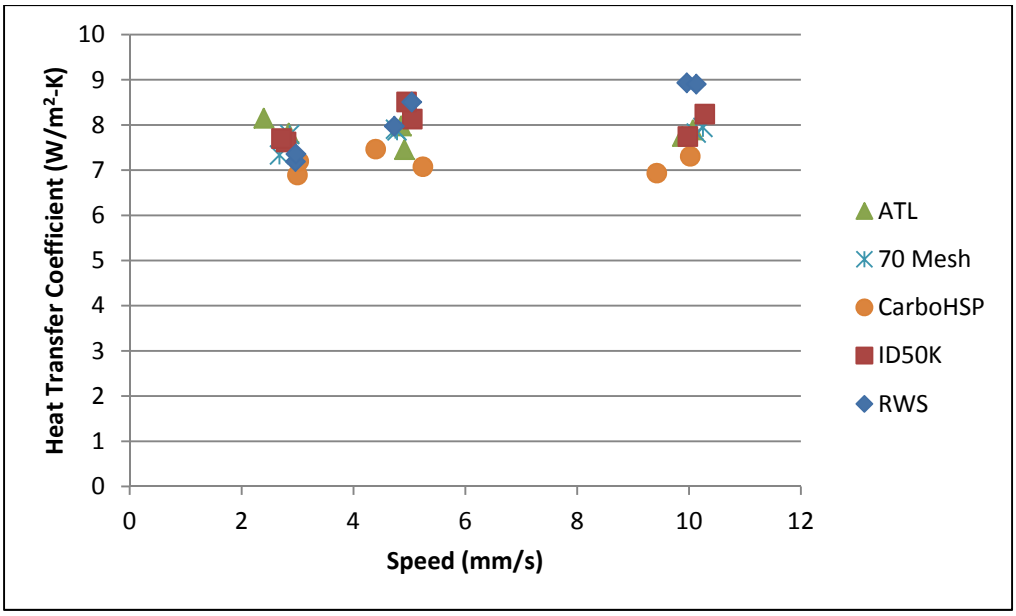

Figure 20: Heat Exchanger Effectiveness for Finned Configuration

The heat exchanger effectiveness was also calculated for the system. The finned tube configuration provides an increase in performance of 7-8 times. The high effectiveness of the finned tube configuration, typically two is enough, justifies the use of finned tubes for similar particulates heat exchangers.

CHAPTER 8

DISCUSSION

The bare tube heat exchanger configuration has shown that the most effective particle for heat transfer in this geometry is the Riyadh White Sand, though not conclusive this sand also has the widest range in variance in the particulate sizes as shown in Appendix C. The values for the heat transfer coefficient ranges from 40 – 120 W/m2-K. These values are within the typically suggested range of the literature as suggested by Brinn (9).

An important note for the data taken is that it corresponds with the superficial speed. That is, the speed is shown as if the cross sectional area is 0.1143 m by 0.1143 m. However, as the sand flows through the module the heaters cause a decrease in the cross sectional area and results in an increase in flow velocity near the tubes. The finned tubes have a larger profile than the bare tubes, so it is important to realize that for the same superficial speed the actual speed near the tubes is higher in the finned case than in the bare tube case.

Attempts to correlate the heat transfer coefficients with their thermal and physical properties have proven inconclusive. The SMD, while important when choosing the geometrical configuration of the heat exchanger does not account for the distribution of the particle size. One important point of investigation would be to observe the effects of having mono-dispersed particulates versus a mixture of different sizes. The Riyadh White Sand had the largest variation in sizes followed closely by the ID50-K both of which were some of the higher performing materials but the results nevertheless remain inconclusive. To counteract this plans have been made to conduct tests using glass ballotoni beads. These beads present a cost effective way to

measure heat transfer properties independent of material composition, and irregular particle shapes.

As seen from Figures 6 and 7 the most effective material in heat transfer ability is the Riyadh White Sand. Though the Riyadh White Sand has the highest heat transfer coefficient it is also one of the more lightly colored sands which affects the absorptivity of the receiver. As such the Accucast ID50-K was ultimately chosen for further development as a heat transfer medium due to its relatively high heat transfer properties, in comparison to the CarboHSP. A finned heat exchanger has been chosen for use as a prototype heat exchanger due to the presence of fins increasing the effective heat transfer coefficient by approximately 8 times.

From the data collected, a set of correlations have been created for the various materials. This correlation is a quadratic fit using the superficial velocity (V) of the particulate. An attempt has been made to correlate the heat transfer coefficient with the thermal conductivity and particle size however a direct relationship could not be found.

$$h = a + b_1 V + b_2 V^2$$

Table 12: Correlations for Bare Tubes

	b_2 Coefficient	b_1 Coefficient	a	R^2
Atlanta Industrial Sand	90.78	3.58	-0.12	1.00
Riyadh White Sand	80.38	5.29	-0.27	0.94
Accucast ID50-K	79.86	5.80	-0.27	0.98
CarboHSP	88.03	2.94	-0.11	0.95
Arizona Fracking Sand	100.22	2.36	-0.05	0.99

Table 13: Correlations for Finned Tubes

	b_2 Coefficient	b_1 Coefficient	a	R^2
Atlanta Industrial Sand	-0.69	12.06	66.54	0.88
Riyadh White Sand	0.32	-2.57	96.38	0.81
Accucast ID50-K	-0.35	7.66	74.04	0.96
CarboHSP	-0.11	3.06	73.51	0.70
Arizona Fracking Sand	-0.83	17.43	50.88	0.99

In order to study the correlation between particle sizes and heat transfer there are plans to run this experiment using mono-disperse glass beads. These glass beads will provide a material that is chemically and geometrically similar across different tests. The bead particle sizes that will be used will closely resemble the particulate sizes that have been used in this paper.

These correlations only apply for particulate temperatures below 150°C. At higher temperatures the pertinent transport properties such as the thermal conductivity of the air and the particulate solid may change somewhat but not as much as pertinent fluid properties such as the viscosity in analogous fluid heat exchngers. Consequently, these low temperature results should be a reasonable first estimate of the heat transfer coefficient at higher temperatures. Additionally, at higher temperatures there will be increased heat transfer due to radiation which will improve the heat transfer perfromance.

CHAPTER 9

CONCLUSION

This experiment shows the heat transfer properties of a variety of materials through both a finned and bare tube heat exchanger. These results have been validated by using air as the thermal medium and comparing the resulting data to classic heat transfer literature. The validation has shown that while there are some turbulence effects due to preceding rows of heaters, the heat exchanger more closely simulates heat transfer over a single tube in cross flow rather than a tube bundle. The following table presents a summary of the heat transfer coefficient values found from this experiment. These values are indirectly used to evaluate the heat transfer of the heat exchanger and are a results of evaluating the heat transfer from a surface to the flowing packed bed of particulates.

Table 14: Summary of the Average Heat Transfer Coefficients for Bare Tubes

Speed	~3mm/s		~5mm/s		~10mm/s	
Power	70-100W	150-180W	70-100W	150-180W	70-100W	150-180W
Accucast ID50-K	100.34	100.14	104.85	106.01	114.17	114.31
Atlanta Industrial Sand	92.31	92.43	102.08	99.04	107.28	104.25
Arizona Fracking Sand	96.70	95.60	103.00	103.60	110.20	110.80
CarboHSP	94.18	96.74	98.84	100.69	105.09	107.10
Riyadh White Sand	106.72	105.36	110.21	111.61	118.87	119.52

Table 15: Summary of the Effective Heat Transfer Coefficients for Finned Tubes

Speed	~3mm/s		~5mm/s		~10mm/s	
Power	70-100W	150-180W	70-100W	150-180W	70-100W	150-180W
Accucast ID50-K	93.77	94.69	107.25	113.26	112.90	123.03
Arizona Fracking Sand	96.35	89.13	102.75	102.27	114.67	117.31
Atlanta Industrial Sand	89.68	93.48	88.00	95.54	101.05	110.85
CarboHSP	78.67	82.90	84.56	88.87	88.75	95.55
Riyadh White Sand	94.17	96.85	110.85	121.10	141.91	141.82

When comparing the two configurations the finned tube configuration has a fin effectiveness of about 8 across the different types of particulate materials. Due to the low cost of fins this is an effective method of increasing the heat transfer.

The data shows that the Riyadh White Sand has been shown to perform consistently as a thermal medium in comparison to the other materials. Accucast ID50-K has also been shown to have the second highest heat transfer coefficient and is a material of interest due to other factors that are not within the scope of this experiment. Unfortunately, a correlation between the flow speed, mean particle size, thermal conductivity and the heat transfer coefficient has been inconclusive. However, correlations for each of the individual materials have been found and can be used for predicting the heat transfer coefficients for larger scale experiments. As such it is recommended that while this data does give a range of expected values for plug flow through a heat exchanger, materials should be individually tested on a small scale prior to large scale experiments. Additionally, these tests only apply at temperatures below 150°C and should still be tested at higher temperatures where the materials properties are expected to change and radiation becomes important.

APPENDIX A

THERMOCOUPLE CALIBRATOINS

Calibrations were completed using a standard platinum resistance thermometer (SPRT) as the calibration standard. The SPRT was calibrated to the international temperature scale of 1990 (ITS-90) by BURNS engineering. This provides a calibration standard ranging from 0°C - 420°C.

To calibrate the thermocouples a water bath is used to circulate the water at a uniform temperature. The heaters with the already attached thermocouples are removed from the heat exchanger and placed within the water bath. This water bath covers from 20°C - 85°C.

At higher temperatures a fluidized bath could not be used. The bath is vigorous enough to destroy the solder and tape used to attach the thermocouples. In addition the thermocouple beads are destroyed as well. The first attempt destroyed FT TC 3, as such the basic omega standard is used for it.

Table 16: Thermocouple Calibration Constants, Uncertainties and Their Range

	U_A	U_B	U_C	Slope	Intercept	Range
BT TC 1	3.01E-03	2.50E-03	3.92E-03	9.97E-01	4.95E-01	Valid for 18°C to 86°C Range
BT TC 2	3.09E-03	2.50E-03	3.98E-03	9.97E-01	4.46E-01	Valid for 18°C to 86°C Range
BT TC 3	5.12E-03	2.50E-03	5.69E-03	9.98E-01	1.87E-01	Valid for 18°C to 86°C Range
BT TC 4	3.15E-03	2.50E-03	4.02E-03	9.97E-01	3.77E-01	Valid for 18°C to 86°C Range
BT TC 5	4.17E-03	2.50E-03	4.86E-03	9.96E-01	3.60E-01	Valid for 18°C to 86°C Range
BT TC 6	3.02E-03	2.50E-03	3.92E-03	9.95E-01	3.29E-01	Valid for 18°C to 86°C Range
Inlet	6.97E-03	1.00E+00	1.00E+00	9.99E-01	2.09E-01	Valid for 18°C to 86°C Range
FT TC 1	1.66E-03	2.50E-03	3.00E-03	1.00E+00	2.51E-02	Valid for 20°C to 87°C Range
FT TC 2	1.59E-03	2.50E-03	2.96E-03	9.99E-01	3.11E-01	Valid for 20°C to 87°C Range
FT TC 3	N/A	N/A	N/A	9.99E-01	3.11E-01	2.2°C Omega Standard
FT TC 4	2.10E-03	2.50E-03	3.27E-03	1.00E+00	5.44E-01	Valid for 20°C to 87°C Range
FT TC 5	2.16E-03	2.50E-03	3.30E-03	1.01E+00	5.40E-01	Valid for 20°C to 87°C Range
FT TC 6	1.32E-03	2.50E-03	2.83E-03	1.00E+00	6.48E-01	Valid for 20°C to 87°C Range

To calibrate the surface temperature thermocouples the entire heater apparatus was dropped into a fluidized bath. The calibration uses a linear fit.

APPENDIX B

UNCERTAINTY TABLES (EES)

The following figures show the uncertainty calculation for the particulate side heat transfer coefficient. The purpose of these figures is to show the major sources of uncertainty in the experiment. U_F is an uncertainty factor of 10% tied to the specific heat. k is the conductivity of the box and is used for heat loss estimation.

$h_{avg,LMTD}$ = 117.9±1.565 [W/m^2-K]

Diameter = 0.01588±0.0001 [m]	$\partial h_{avg,LMTD}/\partial$ Diameter = -7426	22.52 %
Length = 0.1016±0.0001 [m]	$\partial h_{avg,LMTD}/\partial$ Length = -1160	0.55 %
m_1 = 0.6744±0.0001	$\partial h_{avg,LMTD}/\partial m_1$ = -2.657	0.00 %
m_2 = 0.7555±0.0001	$\partial h_{avg,LMTD}/\partial m_2$ = -2.347	0.00 %
m_3 = 0.719±0.0001	$\partial h_{avg,LMTD}/\partial m_3$ = -2.515	0.00 %
N_{tubes} = 8±1.000E-07	$\partial h_{avg,LMTD}/\partial N_{tubes}$ = 0.0006342	0.00 %
q_{total} = 176.2±1.8 [W]	$\partial h_{avg,LMTD}/\partial q_{total}$ = 0.7006	64.94 %
ρ = 0.000001823±1.823E-07 [kg/mm^3]	$\partial h_{avg,LMTD}/\partial \rho$ = 2.649	0.00 %
scan = 310±0.000001	$\partial h_{avg,LMTD}/\partial$ scan = 0	0.00 %
T_1 = 78.15±0.0039	$\partial h_{avg,LMTD}/\partial T_1$ = -0.5028	0.00 %
T_2 = 72.47±0.004	$\partial h_{avg,LMTD}/\partial T_2$ = -0.5028	0.00 %
T_3 = 83.1±0.0057	$\partial h_{avg,LMTD}/\partial T_3$ = -0.5028	0.00 %
T_4 = 77.4±0.004	$\partial h_{avg,LMTD}/\partial T_4$ = -0.5658	0.00 %
T_5 = 69.67±0.0049	$\partial h_{avg,LMTD}/\partial T_5$ = -0.5658	0.00 %
T_6 = 76.64±0.0039	$\partial h_{avg,LMTD}/\partial T_6$ = -0.5658	0.00 %
T_{amb} = 20±5 [C]	$\partial h_{avg,LMTD}/\partial T_{amb}$ = 0.009244	0.09 %
T_{inlet} = 37.68±0.0074 [C]	$\partial h_{avg,LMTD}/\partial T_{inlet}$ = 3.185	0.02 %
$t_{mass,1}$ = 9.91±0.01	$\partial h_{avg,LMTD}/\partial t_{mass,1}$ = 0.1808	0.00 %
$t_{mass,2}$ = 11.22±0.01	$\partial h_{avg,LMTD}/\partial t_{mass,2}$ = 0.158	0.00 %
$t_{mass,3}$ = 10.47±0.01	$\partial h_{avg,LMTD}/\partial t_{mass,3}$ = 0.1727	0.00 %
time = 3100±0.01 [s]	$\partial h_{avg,LMTD}/\partial$ time = 9.057E-09	0.00 %
U_F = 1±0.1	$\partial h_{avg,LMTD}/\partial U_F$ = -5.389	11.86 %
UA = 0.2934±0.02934 [W/K]	$\partial h_{avg,LMTD}/\partial$ UA = -0.6072	0.01 %

Figure 21: Bare Tube Uncertainty Calculation with Individual Variable Uncertainty, Partial Derivative and Percent Weight of Uncertainty

$h = 53.27 \pm 0.35$ [W/m^2-K]		
$anem_{diam} = 4 \pm 0.001$ [in]	$\partial h / \partial anem_{diam} = 0$	0.00 %
$box_{length} = 4.5 \pm 0.001$ [in]	$\partial h / \partial box_{length} = 0$	0.00 %
$D = 0.625 \pm 0.001$ [in]	$\partial h / \partial D = -85.24$	6.05 %
$k_{kapton} = 0.12 \pm 0.012$ [W/m-K]	$\partial h / \partial k_{kapton} = 0$	0.00 %
$L = 4 \pm 0.001$ [in]	$\partial h / \partial L = -13.32$	0.15 %
$OD_{tube,inch} = 0.62 \pm 0.001$ [in]	$\partial h / \partial OD_{tube,inch} = 0$	0.00 %
$Q = 97.33 \pm 0.6096$ [W]	$\partial h / \partial Q = 0.5474$	92.73 %
$speed = 817.1 \pm 8.171$ [ft/min]	$\partial h / \partial speed = 0$	0.00 %
$T_1 = 66.18 \pm 0.0039$ [C]	$\partial h / \partial T_1 = -0.16$	0.00 %
$T_2 = 62.27 \pm 0.004$ [C]	$\partial h / \partial T_2 = -0.3201$	0.00 %
$T_3 = 62.85 \pm 0.0057$ [C]	$\partial h / \partial T_3 = -0.16$	0.00 %
$T_4 = 74.33 \pm 0.004$ [C]	$\partial h / \partial T_4 = -0.1368$	0.00 %
$T_5 = 72.87 \pm 0.0049$ [C]	$\partial h / \partial T_5 = -0.2736$	0.00 %
$T_6 = 63.55 \pm 0.0039$ [C]	$\partial h / \partial T_6 = -0.1368$	0.00 %
$T_{inlet} = 20.33 \pm 0.0425$ [C]	$\partial h / \partial T_{inlet} = 0.5473$	0.45 %
$T_{outlet} = 23.41 \pm 0.0425$ [C]	$\partial h / \partial T_{outlet} = 0.6402$	0.62 %
$time = 3120 \pm 0.01$	$\partial h / \partial time = 0$	0.00 %

Figure 22: Air Validation Uncertainty Calculation with Individual Variable Uncertainty, Partial Derivative and Percent Weight of Uncertainty

APPENDIX C

FURTHER DETAILS ON SIEVING

The sifting device used is a Laboratory Test Sieve Vibrator built by the Derrick Mfg. Co. It is a Model 150, 25-60 cycle, 1/10 H.P., 0-6000 rpm sifter. The sieves are in order from the widest mesh openings to the narrowest with each sieve meeting ASTM E-11 standards. A 100mL beaker is used to take a weighed sample of the material from discharge of the heat exchanger, the material is then placed into the top sieve.

Figure 23: Sifting Device with Stacked Sieves

The sifter is then used to vibrate the particulates such that the smaller particulates have the opportunity to fall through the mesh. The process is run over the course of several minutes until the particulates have settled on the mesh of their corresponding size. After the particulates

have settled, the amount of material on each mesh is measured to see the size distribution of the particles and to measure the Sauter Mean Diameter (SMD).

Table 17: Distribution of Particle Sizes

	SMD (mm)	25	35	50	70
Arizona Fracking Sand	0.26	0%	33%	97%	0%
Atlanta Industrial Sand	0.30	0%	40%	60%	0%
Riyadh White Sand	0.34	16%	67%	31%	0%
ID50-K	0.27	0%	37%	45%	16%
CarboHSP	0.61	65%	32%	0%	0%
Riyadh Red Sand	0.26	0%	10%	90%	0%

APPENDIX D

AIR FLOW UNIFORMITY VALIDATION

To check for air uniformity in the air validation experiment two anemometers were used. The first is an anemometer that encloses the entirety of the inlet area to obtain average flow speed. The second anemometer is a probe that can be used to measure the local air speed. This is placed upstream of the heat exchanger in three different measurement slots. Once inserted into a slot, the probe is used to measure three locations at varying depths to form a 9x9 grid. Table 18 shows the first attempt at measuring the air uniformity.

Table 18: Air Uniformity Table 1st Setup

0.30 ± 0.05	0.53 ± 0.09	0.26 ± 0.11
0.54 ± 0.04	1.00 ± 0.03	0.50 ± 0.08
0.25 ± 0.08	0.50 ± 0.06	0.28 ± 0.09

The tables show the flow speed at each of the locations relative to the maximum flow speed at the center. As can be seen above the airflow outside the central region is greatly reduced due to wall friction.

Table 19: Air Uniformity Table 2nd Setup

0.86 ± 0.01	0.99 ± 0.01	0.99 ± 0.01
0.83 ± 0.01	1.00 ± 0.01	0.91 ± 0.02
0.84 ± 0.02	0.98 ± 0.01	0.92 ± 0.01

Table 19 is measured with the honeycomb structure in place. A slight misalignment in the heat exchanger apparatus led to a slight bias at the top right of the grid. After realigning the setup, the

local air measurements showed an acceptable level of uniformity across the inlet cross-section of the heat exchanger.

Table 20: Air Uniformity Table 3rd Setup

0.87 ± 0.01	0.95 ± 0.01	0.89 ± 0.01
0.84 ± 0.01	1.00 ± 0.01	0.92 ± 0.01
0.86 ± 0.02	0.94 ± 0.01	0.91 ± 0.02

APPENDIX E

TEMPERATURE MIXING

Due to restrictions in the height of the test apparatus a mixed outlet temperature was not achievable. Unlike fluidized beds, slug flow has particulates traveling in a very constrained fashion leading to temperature striations within the particles as shown by Brinn. The same effects could be seen in the attempts to measure the outlet temperature. Readings at the outlet were higher than the average outlet temperature should have been as suggested by control volume analysis. Even a slight displacement of the thermocouple could then cause the thermocouple to read a lower than expected temperature. With the minimal available working area a theoretical calculation was instead used to find the average outlet temperature as can be seen in Chapter 6. Despite that, several attempts have been made to obtain mixed outlet temperatures.

The first design involved the creation of a chute that would redirect the particle flow. The first prototype would use a series of meshes to simultaneously force mixing and allow particulate flow through various layers. The original plan design involved the creation of these slats using 10 x 10 mesh count sized meshes. Unfortunately this allowed too much particulate flow. Other available meshes of higher count did not completely eliminate this problem.

As such the design was simplified for the sake of expediency and to eliminate excess heat loss fin surfaces. The walls are made up of Duraboard (38) which is a high temperature fiber insulation board.

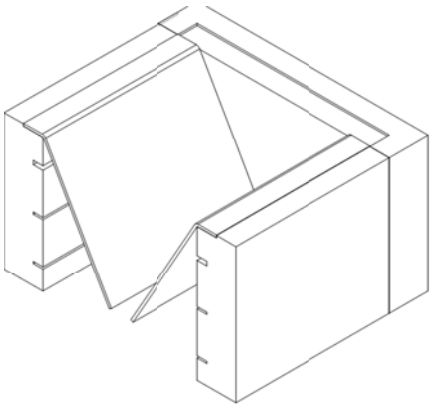

Figure 24: Mixer Unit Without Front Wall

Figure 24 shows a single designed section, the mixer will use four of these sections with each successive section perpendicular to the next section. The use of four mixing sections has achieved adequate mixing for on sun testing using the Georgia Tech High Flux Solar Simulator.

REFERENCES

1. National Renewable Energy Laboratory. *Engineering Evaluation of a Molten Salt HTF .* [Online] http://www.nrel.gov/csp/troughnet/pdfs/ulf_herrmann_salt.pdf.

2. Concentrating Solar Power. *Solar Energy Development Programmatic EIS.* [Online] http://solareis.anl.gov/guide/solar/csp/.

3. *Heat and Flow Characteristics of Packed Beds .* **Achenbach, E.** New York : Elsevier Science Inc, 1995.

4. *Heat transfer in moving beds with a stagnant .* **Molerus, Otto.** 1996.

5. *Discrete Modeling of Heat Conduction in Granular Media.* **Vargas-Escobar, Watson.** Pittsburgh : s.n., 2002.

6. *Conductivity of granular media with stagnant interstitial fluids via thermal particle dynamics simulation.* **Watson L. Vargas, J.J. McCarthy.** Pittsburgh : s.n., 2001.

7. *Heat transfer in rotary kilns with interstitial gases.* **Shi, Deliang, Vargas, Watson and McCarthy, J.J.** Piittsburgh : s.n., 2008.

8. *HEAT TRANSFER IN FLOWING PACKED BEDS .* **Denloye, A and Botterill, J.** England : Chemical Engineering Science, 1976, Vol. 32. 463-465.

9. *Heat Transfer to Granular Materials: Settled Beds Moving Downward through Vertical Tubes .* **M. S. BRINN. S. J. FRIEDMAN, F.A. GLUCKERT, R.L. Pigford.** 6, s.l. : Industrial and Chemical Engineering, 1948, Vol. 40. 1050-1061.

10. *Experimental Study of a Sand–Air Heat Exchanger for Use With a High-Temperature Solar Gas Turbine System.* **Alrished, A, et al., et al.**

11. *Study on Solid Particles as a Thermal Medium.* **Nguyen, C, et al., et al.** s.l. : Elsevier, Vol. 49.

12. KD2 Pro. *Decagon Devices.* [Online] http://www.decagon.com/products/thermal/instruments/KD-2-Pro-Thermal-Properties-Analyzer/?utm_source=reorg.

13. *Heat transfer and flow characteristics around a finned-tube bank heat.* **Honda, Ryosuke, Umekawa, Hisashi and Ozawa, Mamoru.** s.l. : Nuclear Instruments and Methods in Physics Research A, 2009. 188-191.

14. *Surface-to-bed heat transfer influidised beds offine particles.* **Natale, Francesco, Lancia, Amedeo and Nigro, Roberto.** Napoli : May 2009.

15. *CONVECTIVE HEAT TRANSFER PERFORMANCE OF SAND FOR THERMAL ENERGY STORAG.* **Golob and M.** s.l. : Georgia Institute of Technology.

16. **McAdams, William.** *Heat Transmission.* New York : s.n.

17. *ASHRAE HandBook.* New York : American Society of Heating, Refrigeration and Air Conditioning Engineers, Inc., 1977.

18. *The granular silo as a continuum plastic flow: The hour-glass vs the clepsydra.* **Staron, L, Lagreee, P and Popinet, S.** s.l. : AIP Physics of Fluids.

19. *Investigations of the Specific Heat of Solid Bodies.* **Kopp, Herman.** s.l. : Royal Society Publishing, 1865.

20. *Application of Neumann–Kopp rule for the estimation.* **Leitner, J, et al., et al.** 13, s.l. : Thermochimica Acta, Vol. 7.

21. *EXPERIMENTAL STUDY OF A SAND-AIR HEAT EXCHANGER FOR USE WITH A HIGH TEMPERATURE SOLAR GAS TURBINE SYSTEM.* **A. Alrished, H. Al-Ansary, S. I. A.-K., S. I D. Sadowski, A. El_Leathy, Z. Al-Suhaibani.**

22. High-Temperature Cartridge Heater 120 Volts, 5/8" Dia, 4" Length, 200 Watts. *McMaster-Carr.* [Online] McMaster-Carr, 2012. http://www.mcmaster.com/#3618k114/=xxs66s.

23. GPM 8212. *Bench-Top AC Power Meter, GPM-8212.* [Online] GwinStek. http://www.gwinstek.com/en-global/products/Other_Meters/AC_Power_Meters/GPM-8212.

24. Finned Tubing. *Heat Exchange Applied Technology.* [Online] http://www.heat-voss.com/finned-tubing.html.

25. Ultem. *Gemini Plastics.* [Online] 2012. http://www.gplastics.com/pdf/ultem.pdf.

26. 34970A Data Acquisition / Data Logger Switch Unit. [Online] http://www.keysight.com/en/pd-1000001313:epsg:pro-pn-34970A/data-acquisition-data-logger-switch-unit?&cc=US&lc=eng.

27. *Material Safety Data Sheet.* s.l. : Carbo Ceramics, 2007.

28. Quartz. *National Institute of Standards and Technology.* [Online] http://webbook.nist.gov/cgi/cbook.cgi?ID=C14808607&Type=JANAFS&Table=on.

29. Hematite. *National Institute of Standards and Technology.* [Online] http://webbook.nist.gov/cgi/cbook.cgi?ID=C1317608&Type=JANAFS&Table=on.

30. Ruitle (TiO2). *National Institute of Standards and Technology.* [Online] http://webbook.nist.gov/cgi/cbook.cgi?ID=C1317802&Mask=2.

31. aluminium oxide. *National Institute of Standards and Technology.* [Online] http://webbook.nist.gov/cgi/cbook.cgi?ID=C1344281&Type=THZ-IR-SPEC&Index=0.

32. Ultra Precise RTD Sensors for Industrial Application. *Omega.* [Online] Omega. http://www.omega.com/pptst/P-Ultra_RTD.html.

33. AirFlow LCA 30VT. *TSI.* [Online] http://www.tsi.com/uploadedFiles/_Site_Root/Products/Literature/Manuals/lca.pdf.

34. Calibratio Services. *Burns Engineering.* [Online] http://www.burnsengineering.com/calibration.

35. **Incropera, Frank and Dewitt, David.** *Fundamentals of Heat and Mass Transfer.* New York : John Wiley & Sons, 2002. pp. 426,438-441.

36. Omega Thermocouple Accuracy and Color Codes. *Omega.* [Online] http://www.omega.com/toc_asp/frameset.html?book=Temperature&file=tc_colorcodes.

37. **Kline, S and McClintock, F.** *Describing the uncertainties in single sample experiments.* 1953.

38. Duraboard HD. *Unifrax.* [Online] https://www.unifrax.com/web/UnifraxHome3.nsf/HTMLNews/F8A7EDDED0B3BA1E85256C3E0060278D?OpenDocument.

39. *GAS CHANNELLING AND HEAT TRANSFER IN MOVING.* **CRAWSHAW, J. P., PATERSON, W. R. and SCOTT, D. M.**

40. *Convective heat transfer to rapidly .* **Patton, J.S, Sabersky, R.H. and Brennen, C.E.** 8, Pasadena : Ins. J. Heat Mass Transfer, 1986, Vol. 29.

41. *Heat transfer and bubble characteristics in a fluidized bed.* **Kim, Sung Won, et al., et al.** s.l. : International Journal of Heat and Mass Transfer, 2003, Vol. 46. 399-409.

42. *Packed-bed thermal storage for concentrated solar power – Pilot-scale demonstration and industrial-scale design.* **Zanganeh, G., et al., et al.** s.l. : Solar Energy, 2012. 3084-3098.

43. *A theoretical analysis of heat transfer due to particle Impact.* **Sun, J. and Chen, M.** Urbana : Int J. Heat Mass Transfer, 1987.

44. *Modeling of heat transfer processes in particulate .* **Süle, Zoltán , Mihálykó, Csaba and Lakatos, Béla G.** Veszprém : 9th International Symposium on Process Systems Engineering, 2006.

45. **Incropera, Frank and Dewitt, David.** *Fundamentals of Heat and Mass Transfer.* New York : John Wiley & Sons, 2002.

46. Concentrating Solar Power (CSP) Technologies. *Solar Energy Development Programmatic EIS.* [Online] [Cited: June 25, 2013.] http://solareis.anl.gov/guide/solar/csp/.

47. Ultem. *Gemini Plastics Inc.* [Online] [Cited: 6 26, 2013.] http://www.gplastics.com/pdf/ultem.pdf.

48. **Keysight Technologies.** 34970A Data Acquisition / Data Logger Switch Unit. *Keysight Technologies.* [Online] May 2012. http://www.me.umn.edu/courses/me4331/FILES/AgilentManual_34.pdf.